Chemical Engineering Journal 97 (2004) 47–67

Chemical Engineering Journal

www.elsevier.com/locate/cej

Liquid pipeline leak detection system: model development and numerical simulation

Kingsley E. Abhulimen, Alfred A. Susu*

Chemical Engineering Department, University of Lagos, Lagos, Nigeria

Abstract

A new model to detect leaks optimally in liquid pipelines is presented. The model uses the concept based on the Liapunov stability criteria to evolve a criterion for pipeline leak detection. A flow model was derived for a typical pipeline flow system, and the inclusion of leak factor k_L in the flow model gives an indication of the relative degree of deviation from equilibrium or no leak situation. The numerical solution by the implicit finite difference scheme was used to solve the transient second-order partial differential equations describing the flow process. A set of parametric velocity and pressure profiles were generated and validated using industry data. A stability matrix, useful for determining the eigenvalues (λ's), evolves from the deviation model of velocity and pressure. A leak is detected whenever any of the eigenvalues is less than -1, whereas a surge in the pipeline is detected whenever any of the eigenvalues is greater than 1. The simulation profiles of eigenvalues of a crude oil transporting pipeline segment, of a pipeline network of an operating oil company in the Niger Delta region of Nigeria, show that pressure deviations are more sensitive parameter for leak detection than volume deviations. Volume deviations appear to be good indicators for larger leak systems. Single leak situation as well as double leak situations in a pipeline system were analyzed and discussed.

Keywords: Liquid pipelines; Leak detection system; Numerical simulation

1. Introduction

Most of the conventional leak detection systems to date, have in general failed to perform optimally within the criteria of response time, robustness, reliability, sensitivity, accuracy and cost. A leak detection system, by itself, has no effect on the technical integrity of the pipeline as it is only installed to make the operator aware of a leak in order for the operator to manage the risk of pipeline failure [14]. Several pipeline leak detection technologies are based on the continuous analysis of pipeline pressure, temperature, flow and density [11].

A number of models exist in the literature for leak detection. The mass balance model, though a reliable method, has been found to fail as a sensitive and fast leak detection system. The key factor in its popularity is its simplicity [8]. The dynamic model is more complicated. This model attempts to mathematically model fluid flow within a pipeline. It uses hydraulic equation with actual pipeline data to develop expected hydraulic profile. A leak is suspected when there exist discrepancy patterns between measured and calculated flow; a leak is then declared once a discrepancy pattern specific to a leak is recognized [3,4,7,9]. This model fallout because of its mathematical complexity, its inherent thresholds, its dependability on the accuracy and availability of wide range of instrumentation and its extensive data requirement [17]. Hence, this form of leak detection is exposed to a high number of potential false alarms.

The pressure deviation model seems to be the most predictive leak detection method. For example, pressure deviation can detect relatively small leaks in noisy signal in relative environment within a time period of between 3 and 8 min after a surge reaches the monitors. Also, pressure point analysis only operates during steady-state pipeline conditions. However, the pressure point analysis method has not been too successful on large transmission pipelines [10].

We present here a new leak detection model that is universally applicable to all pipeline/fluid systems. The model is based on the Liapunov criteria for stability systems. A leak is detected whenever the evaluated eigenvalues generated from the derived stability flow matrix (i.e. the Jacobean of pressure and velocity measurements in time, at specific sensor spacing) is less than -1. Specifically, the velocity and pressure measurements are converted to dimensionless variables over an equilibrium value (V_E, P_E) to account for error associated with transients at upstream of sensors. Optimal leak detection performance is obtained with this model since only flow or pressure changes are required rather than precise instrument measurements. The proposed methodology

* Corresponding author. Tel.: +234-820311x491.

1385-8947/$ – see front matter © 2003 Elsevier B.V. All rights reserved.
doi:10.1016/S1385-8947(03)00098-6

Nomenclature

A	fluid dimensionless constant
A_c	cross-sectional area (m^2)
b_1	parameter constant
c	sonic velocity (m/s)
C	fluid dimensionless constant
d_c	critical hole diameter
D	diameter of pipe (m)
D_{LD}	leak detection length downstream (m)
D_{LU}	leak detection length upstream (m)
E_s	Young's modulus of steel 210E9 (Pa)
f	friction factor
G	mass velocity (kg/s m^2)
H	enthalpy (J/kg)
H_0	inlet enthalpy (J/kg)
H_L	enthalpy of leaking fluid (J/kg)
k	friction factor constant
k_L	leak detection factor
K	pipeline separation losses
K_b	bulk modulus constant
K_{eff}	effective pipe constant
K_{j+i}	separation constant at j and i node
L	pipe length (m), mixing length parameter, Prandtl mixing length
L_0	pipe length (m)
L_R	leak rate (kg/s)
M	mass rate (kg/s)
M_e	mass rate at equilibrium (kg/s)
n	counter
P	pressure (bar)
P_e	pressure at equilibrium (bar)
P_{in}	inlet pressure (bar)
P_{out}	outlet pressure (bar)
P_0	initial pressure (bar)
R	radial distance (m)
S.D.(λ_{ij})	standard deviation of eigenvalue
t_w	pipe wall thickness (m)
Δt_u	time lag for upstream side
Δt_d	time lag for downstream side
T	time (s), fluid temperature (K)
T_0	inlet temperature (K)
u	velocity of gas (m/s)
U	heat transfer coefficient (J/kg K)
V	molar volume (m^3/mol)
V_e	velocity in equilibrium (m/s)
V_{j+1}	velocity at grid $j+1$ (m/s)
V_L	velocity of leak (m/s)
V_Z	velocity in Z-direction (m/s)
V_0	initial velocity (m/s)
$\bar{V}_Z$	dimensionless velocity
Z	pipeline length (m)

Greek symbols

γ	pressure error function
γ_{fluid}	fluid parameter variable
ε	velocity error function
ζ_k	deviation function at the forward time
η	mass error function
H	Jacobean matrix
λ_{ij}	eigenvalues (roots)
μ	viscosity
ξ	compressibility factor
ρ	density of fluid (kg)
τ	shear stress (N/m^2)
φ	gas constant parameter
Ω_k	deviation function at the present time

is proactive to changes in pipeline, detects faster as it simulates on real time the changes in velocity and pressure. This method has been applied to the some pipeline segment of an Oil Company operating in the Niger Delta region of Nigeria. The simulation plots shows that pressure measurements are more sensitive parameters for leak detection than volume measurements.

2. Model development and numerical simulation for liquid pipeline flow systems

2.1. Modeling development

Eq. (1) describes a second-order, non-linear partial differential equation useful for describing isothermal transient flow systems. The model equation was developed using the Navier–Stokes momentum balance equation, the steady-state energy equation and the Prandtl correlation for turbulence shear stress [2]:

$$2\gamma_{fluid}\left(\frac{\partial V_Z}{\partial r}\right)\left(\frac{\partial^2 V_Z}{\partial r^2}\right)+\left(\frac{\gamma_{fluid}}{r}\right)\left(\frac{\partial V_Z}{\partial r}\right)^2 - F(V_Z)\left(\frac{\partial \rho V_Z}{\partial Z}\right)=\left(\frac{\partial \rho V_Z}{\partial t}\right) \quad (1)$$

where

$$\gamma_{fluid}=\alpha_T+\alpha_L \quad (2)$$

$$\alpha_T=\rho l^2 \quad (3)$$

$$\alpha_L=G\left(n,\frac{\partial V}{\partial Z},k\right) \quad (4)$$

For incompressible flow with a high bulk modulus, Eq. (1):

$$(2\gamma_{fluid\,1})\left(\frac{\partial V_Z}{\partial r}\right)\left(\frac{\partial^2 V_Z}{\partial r^2}\right)+\left(\frac{\gamma_{fluid\,1}}{r}\right)\left(\frac{\partial V_Z}{\partial r}\right)^2 - F(V_Z)\left(\frac{\partial V_Z}{\partial z}\right)=\left(\frac{\partial V_Z}{\partial t}\right) \quad (5)$$

where

$$\gamma_{\text{fluid 1}} = \frac{\alpha_T + \alpha_L}{\rho} \tag{6}$$

$$F(V_Z) = (2K\Psi_Z + b_1\Psi_Z^{-(n+1)}) \tag{7}$$

$$K = 0.5\left(f\frac{Z}{D} + \sum_i eV_i\right) \tag{8}$$

$$f = k_1 + k_2\frac{1}{Nr\,e^{-n}} \tag{9}$$

$$b_1 = -nk_2\left(\frac{2L}{D}\right)\left(\frac{\rho D}{\mu}\right)^{-n} \tag{10}$$

f, the friction factor, is evaluated by any suitable correlation and $\sum_i eV_i$ is the summation of all separation losses. We have used a correlation developed by Shell [13] for evaluating f that is applicable for simplified turbulent flow equation (9). k_2 and n are constants specified for the fluid system by empirical augments. The basic assumptions for the flow model presented in Eq. (5) are: (i) fluid turbulence is given by the Prandtl's mixing length correlation [12,15], (ii) incompressibility fluid system, (iii) isothermal conditions and (iv) no pump work. The dimensionless form of Eq. (5) is given by the following equation:

$$2A\left(\frac{\partial\Psi_Z}{\partial\Re}\right)\left(\frac{\partial^2\Psi_Z}{\partial\Re^2}\right) + (A)\left(\frac{\partial\Psi_Z}{\partial\Re}\right)^2 - (BF(\Psi_Z))\left(\frac{\partial\Psi_Z}{\partial\mathbf{Z}}\right) = (C)\left(\frac{\partial\Psi_Z}{\partial\tau}\right) \tag{11}$$

where

$$A = \frac{l^2}{R^2}, \quad B = \left(\frac{R}{Z_n}\right), \quad C = \left(\frac{\nu R}{Z_n^2 V_{Z_0}}\right), \quad \Re = \frac{r}{R}, \quad \Psi = \frac{Z}{Z_n}, \quad \tau = \frac{\nu t}{Z_n^2}, \quad \Psi_Z = \frac{V_Z}{V_{Z_0}} \tag{12}$$

At steady-state condition, Eq. (11) is further simplified to give the following equation:

$$2A\left(\frac{\partial\Psi_Z}{\partial\Re}\right)\left(\frac{\partial^2\Psi_Z}{\partial\Re^2}\right) + (A)\left(\frac{\partial\Psi_Z}{\partial\Re}\right)^2 - BF(\Psi_Z)\left(\frac{\partial\Psi_Z}{\partial\mathbf{Z}}\right) = 0 \tag{13}$$

The continuity equation describing mass balance for compressible flow systems within the pipeline is presented in the following equation:

$$\frac{\partial\rho}{\partial t} + V_Z\frac{\partial\rho}{\partial Z} + \rho\frac{\partial V_Z}{\partial Z} = 0 \tag{14}$$

The dimensionless form for Eq. (14) is given in Eq. (16) by substituting the dimensionless variables of the following equation:

$$\wp = \frac{\rho}{\rho_0}, \quad \mathbf{Z} = \frac{Z}{Z_z}, \quad \tau = \frac{V_{Z_0}t}{Z_n} \tag{15}$$

The resulting dimensionless equation is shown in the following equation:

$$\frac{\partial\wp}{\partial\tau} + \Psi_Z\frac{\partial\wp}{\partial\mathbf{Z}} + \wp\frac{\partial\Psi_Z}{\partial\mathbf{Z}} = 0 \tag{16}$$

We now present a model to describe the flow behavior of liquid pipeline leak systems. This model was derived by introducing a factor k_L, into the flow model equation (Eq. (11)) and the continuity equation (Eq. (16)), to give Eqs. (17) and (18) which are model equations for flow leak and mass leak, respectively:

$$2A\left(\frac{\partial\Psi_Z}{\partial\Re}\right)\left(\frac{\partial^2\Psi_Z}{\partial\Re^2}\right) + (A)\left(\frac{\partial\Psi_Z}{\partial\Re}\right)^2 - (BF(\Psi_Z))\left(\frac{\partial\Psi_Z}{\partial\mathbf{Z}}\right) = (C + k_{L1})\left(\frac{\partial\Psi_Z}{\partial\tau}\right) \tag{17}$$

$$\frac{\partial\wp}{\partial\tau} + \Psi_Z\frac{\partial\wp}{\partial\mathbf{Z}} + \wp\frac{\partial\Psi_Z}{\partial\mathbf{Z}} = k_L\wp\Psi_L \tag{18}$$

C in Eq. (17) becomes zero when line pack considerations are negligible. k_{L1} represents a measure of the degree of instability which assumes a negative value for a leaking pipeline system. For incompressible fluid, the mass model presented in Eq. (18) becomes:

$$\wp\frac{\partial\Psi_Z}{\partial\mathbf{Z}} = (\wp k_L\Psi_L) \tag{19}$$

FRED model, Fred Model Version 2 [18] is a model that allows the calculation of the potential leak rate in liquid pipelines given by the use of Eq. (20). Further details can be obtained from Shell standards DEP publications:

$$L_R = 0.61\rho\frac{A_c}{10^6}\sqrt{2\left[\frac{10^5(P_{in} - P_{out})}{\rho}\right]} \tag{20}$$

where A_c is the cross-sectional area of the leak hole, given by the following equation:

$$A_c = \tfrac{1}{4}(\pi d_c^2) \tag{21}$$

d_c is the diameter of the leak hole; 0.61 the assumed discharge coefficient of the hole (orifice). P_{in} is the fluid (gauge) pressure in the pipeline, including any static head pressures. P_{out} the back pressure gauge outside the pipeline, which can be evaluated by the following equation:

$$P_{out} = \left(\frac{1025 \times 9.81 \times h}{10^5}\right) \tag{22}$$

h is the water depth and ρ the fluid density. The velocity V_L of the liquid pipeline is given by the following equation:

$$V_L = \frac{L_R}{\rho A_c} = \frac{0.61}{10^6}\sqrt{2\left[\frac{10^5(P_{in} - P_{out})}{\rho}\right]} \tag{23}$$

Once V_L is known, Eqs. (18) and (19) can then be solved.

2.2. Numerical simulation

Eq. (17) is a transient partial differential equation for a pipeline leaking system in (r, z) coordinates. We propose a hypothesis that allows the partial differential equation presented in Eq. (17) in (r and z) to be resolved in the z-axial direction only. This can be derived by transforming the radial component of flow into the axial component of flow. Using $\tan\theta$ as a measure of the relative magnitude of molecular momentum flux in radial direction to convective momentum flux in axial direction (see Eq. (24)):

$$\frac{\partial \Psi_Z}{\partial \Re} = \tan\theta \frac{\partial \Psi_Z}{\partial \mathbb{Z}} \tag{24}$$

Hence Eq. (17) can be transformed to Eq. (25) by substituting Eq. (24) into Eq. (17):

$$2A\tan^3\theta \left(\frac{\partial \Psi_Z}{\partial \mathbb{Z}}\right)\left(\frac{\partial^2 \Psi_Z}{\partial \mathbb{Z}^2}\right) + (A\tan^2\theta)\left(\frac{\partial \Psi_Z}{\partial \mathbb{Z}}\right)^2 - (BF(\Psi_Z))\left(\frac{\partial \Psi_Z}{\partial \mathbb{Z}}\right) = (C + k_L)\left(\frac{\partial \Psi_Z}{\partial \tau}\right) \tag{25}$$

The implicit finite difference scheme is now used to discretize Eq. (25). The implicit formulation is represented by the following equation:

$$2A\tan^3\theta \left(\frac{\Psi_{j+1}^{n+1} - \Psi_j^{n+1}}{\Delta \mathbb{Z}}\right)\left(\frac{\Psi_{j+1}^{n+1} - 2V_j^{n+1} + \Psi_{j-1}^{n+1}}{\Delta \mathbb{Z}}\right) + A\tan^2\theta \left(\frac{\Psi_{j+1}^{n+1} - \Psi_j^{n+1}}{\Delta \mathbb{Z}}\right)^2 - (BF(V_j^{n+1}))\left(\frac{\Psi_{j+1}^{n+1} - \Psi_j^{n+1}}{\Delta \mathbb{Z}}\right) = (C + k_{L1})\left(\frac{V_j^{n+1} - V_j^n}{\Delta \tau}\right) \tag{26}$$

Rearranging Eq. (26), results in final implicit formula presented as the following equation:

$$\Psi_j^n = \Psi_j^{n+1} - \frac{\Delta\tau}{C + k_{L1}}\left(2A\tan^2\theta\left(\frac{\Psi_{j+1}^{n+1} - \Psi_j^{n+1}}{\Delta \mathbb{Z}}\right) \times \left(\frac{\Psi_{j+1}^{n+1} - 2V_j^{n+1} + \Psi_{j-1}^{n+1}}{\Delta \mathbb{Z}}\right) + A\tan^2\theta\left(\frac{\Psi_{j+1}^{n+1} - \Psi_j^{n+1}}{\Delta \mathbb{Z}}\right)^2 - (BF(V_j^{n+1}))\left(\frac{\Psi_{j+1}^{n+1} - \Psi_j^{n+1}}{\Delta \mathbb{Z}}\right)\right) = \Psi_j^{n+1} + \frac{\Delta\tau}{C + k_{L1}}(BF(V_j^{n+1}))\left(\frac{\Psi_{j+1}^{n+1} - \Psi_j^{n+1}}{\Delta \mathbb{Z}}\right) \tag{27}$$

If convective flow transport dominates to make the effect of molecular transport in radial direction negligible, then, $\tan\theta$ becomes zero and Eq. (27) becomes:

$$\Psi_{j+1}^{n+1} = \Psi_j^{n+1} - (\Delta \mathbb{Z})\left(\frac{C + k_{L1}}{BF(V_j^{n+1})}\right)\left(\frac{\Psi_j^{n+1} - \Psi_j^n}{\Delta \tau}\right) \tag{28}$$

$$j = 1, \ldots, n, \qquad k = 1, \ldots, n \tag{29}$$

Similarly, the steady flow model presented in Eq. (13) can also be handled as in Eq. (24) by transforming radial coordinate system to axial system. Hence Eq. (13) can be rewritten to give the following equation:

$$2A(\tan\theta)^2\left(\frac{\partial \Psi_Z}{\partial \mathbb{Z}}\right)\left(\frac{\partial^2 \Psi_Z}{\partial \mathbb{Z}^2}\right) + (A\tan^2\theta)\left(\frac{\partial \Psi_Z}{\partial \mathbb{Z}}\right)^2 - (BF(\Psi_Z))\left(\frac{\partial \Psi_Z}{\partial \mathbb{Z}}\right) = 0 \tag{30}$$

The modified Euler, a predictor–corrector method, can be used to solve the steady-state flow model, as it gives faster convergence, stability, and fairly accurate solutions. The velocity at each node is easily obtained from

$$V_{j+1} = V_0 \Psi_{j+1} \tag{31}$$

The pressure model is obtained from the energy balance equation. The model takes account of separation loss factors thus

$$P_{j+1} = P_0 - \rho V_{j+1}^2 \sum_{j=0}^{j+1} K_{j+1} \tag{32}$$

where K_{j+1} is the separation factor losses up to $j+1$ node.

3. Theory of stability and instability of the flow system

The model to detect leaks in a pipeline is derived by the application of the theory of stability or instability of equilibrium flow systems [16]. Suppose that a pipeline is divided into n-nodes with the defining parameters at each node as $Y_1, Y_2, \ldots, Y_N$. If $Y_1', Y_2', \ldots, Y_N'$ are disturbances or derivatives of the function $Y_1, Y_2, \ldots, Y_N$, and assuming that $Y_1, Y_2, \ldots, Y_N$ are linearly dependent, a system of equation evolves:

$$\begin{aligned} Y_1' &= F_1(Y_1, Y_2, \ldots, Y_N), \\ Y_2' &= F_2(Y_1, Y_2, \ldots, Y_N), \ldots, \\ Y_n' &= F_n(Y_1, Y_2, \ldots, Y_N) \end{aligned} \tag{33}$$

At equilibrium, a point in the pipeline flow vector space $P_E(Y_1^E, Y_2^E, \ldots, Y_N^E)$ has $F_I(Y_1^E, Y_2^E, \ldots, Y_N^E) = 0$ for all $i = 1, \ldots, N$. Hence, a flow system is at equilibrium if the vector flow space function remains the same for all future times. If there is a perturbation, represented by a point P in the neighborhood P_E, Liapunov equilibrium states that for every neighborhood U of P_E in the flow space, there exists a

small neighborhood U_1, which will remain in U for all $t > 0$. If all solutions tend to equilibrium as t tends to infinity, then P_E is said to be asymptotically stable. Conversely a local perturbation like a leak moves the equilibrium from rest, making P_E unstable. Therefore, a system is said to be structurally stable if for any sufficiently small perturbation of the defining equation, the resulting flow is topological equivalent to the initial one. The vector field $F(x)$ of the whole phase portrait for all individual function $f(x)$ at the designated nodes is described by the matrix:

$$\begin{bmatrix} Y_1' \\ Y_2' \\ \vdots \\ Y_N' \end{bmatrix} = \begin{bmatrix} 0 \\ 0 \\ \vdots \\ 0 \end{bmatrix} \tag{34}$$

Hence a perturbed vector $G(x)$ of the same space in the neighborhood of radius $\in$ of $F(x)$ is the same field if $F(x) - G(x) < \in$ rendering the flow a stable one. The sketch below illustrates the concept pictorially where a disturbance $D(x)$ moves the vector field $F(x)$ to another vector field position $G(x)$:

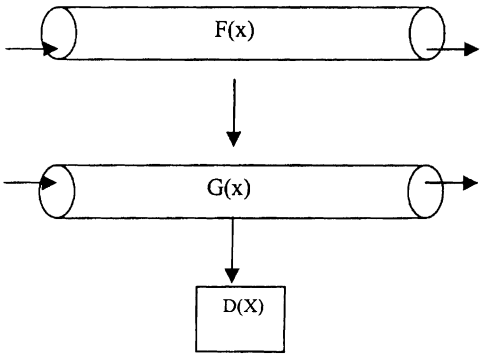

4. Application of stability or instability flow systems in leak detection model

The concept of stability and instability of flow systems (Liapunov equilibrium stability criteria) was applied to a transient flow system, to evolve a model for leak detection. The two-dimensional invertible maps in time and space domain for the flow system is $\tau \to z$, t, and are presented for velocity, pressure and mass changes, in Eqs. (35)–(37), respectively.

$$V_{i+1j} = F_1[V_{ij}, M_{ij}, P_{ij}] \tag{35}$$

$$M_{i+1j} = F_2[V_{ij}, M_{ij}, P_{ij}] \tag{36}$$

$$P_{i+1j} = F_3[V_{ij}, M_{ij}, P_{ij}] \tag{37}$$

where V_{ij}, M_{ij}, P_{ij} are the velocity, mass and pressure at j space node and i time domain, respectively. An equilibrium point can be defined as the domain of stability where, pressure, velocity and mass changes are steady, therefore, $V_{ij} = V_{Ej}$, $M_{ij} = M_{Ej}$, $P_{ij} = P_{Ej}$ are fixed equilibrium points. The velocity, mass, and pressure are measured on real time at the sensors. The velocity and pressure profiles within the pipeline can be simulated using a suitable numerical technique to solve the flow or leak model of Eq. (25). For completely stable flow systems:

$$V_{i+1j} = V_{ij} = V_{Ej} \tag{38}$$

$$M_{i+1j} = M_{ij} = M_{Ej} \tag{39}$$

$$P_{i+1j} = P_{ij} = P_{Ej} \tag{40}$$

$$V_{Ej} = F_1[V_{Ej}, M_{Ej}, P_{Ej}] \tag{41}$$

$$M_{Ej} = F_2[V_{Ej}, M_{Ej}, P_{Ej}] \tag{42}$$

$$P_{Ej} = F_3[V_{Ej}, M_{Ej}, P_{Ej}] \tag{43}$$

Change resulting from a movement from equilibrium state is presented in the following equations:

$$\begin{aligned} V_{i+1j} &= V_{Ej} + \xi_{i+1j} \\ &= F_1[V_{Ej} + \xi_{ij}, M_{Ej} + \eta_{ij}, P_{Ej} + \gamma_{ij}] \end{aligned} \tag{44}$$

$$\begin{aligned} M_{i+1j} &= M_{Ej} + \eta_{i+1j} \\ &= F_2[V_{Ej} + \xi_{ij}, M_{Ej} + \eta_{ij}, P_{Ej} + \gamma_{ij}] \end{aligned} \tag{45}$$

$$\begin{aligned} P_{i+1j} &= P_{Ej} + \gamma_{i+1j} \\ &= F_3[V_{Ej} + \xi_{ij}, M_{Ej} + \eta_{ij}, P_{Ej} + \gamma_{ij}] \end{aligned} \tag{46}$$

Expanding the dimensionless form of Eqs. (44)–(46), using Taylor series and considering only the linear part, results in a system of equation presented below:

$$\xi_{i+1j} = A\xi_{ij} + B\eta_{ij} + C\gamma_{ij} \tag{47}$$

$$\eta_{i+1j} = D\xi_{ij} + E\eta_{ij} + F\gamma_{ij} \tag{48}$$

$$\gamma_{i+1j} = G\xi_{ij} + H\eta_{ij} + I\gamma_{ij} \tag{49}$$

The above equations are composed into the following dimensional matrix equation:

$$\zeta_{i+1j} = H\Omega_{ij} \tag{50}$$

where

$$\Omega_{ij} = \begin{bmatrix} \xi_{ij} \\ \eta_{ij} \\ \gamma_{ij} \end{bmatrix}, \qquad \zeta_{i+1j} = \begin{bmatrix} \xi_{i+1j} \\ \eta_{i+1j} \\ \gamma_{i+1j} \end{bmatrix} \tag{51}$$

$$\begin{aligned} H &= \begin{bmatrix} A & B & C \\ D & E & F \\ G & H & I \end{bmatrix} \\ &= \begin{bmatrix} \left(\frac{\partial F_1}{\partial \mathbf{V}_Z}\right)_{ij} & \left(\frac{\partial F_1}{\partial \mathbf{M}_Z}\right)_{ij} & \left(\frac{\partial F_1}{\partial \mathbf{P}}\right)_{ij} \\ \left(\frac{\partial F_2}{\partial \mathbf{V}_Z}\right)_{ij} & \left(\frac{\partial F_2}{\partial \mathbf{M}_Z}\right)_{ij} & \left(\frac{\partial F_2}{\partial \mathbf{P}}\right)_{ij} \\ \left(\frac{\partial F_3}{\partial \mathbf{V}_Z}\right)_{ij} & \left(\frac{\partial F_3}{\partial \mathbf{M}_Z}\right)_{ij} & \left(\frac{\partial F_3}{\partial \mathbf{P}}\right)_{ij} \end{bmatrix} = JF \end{aligned} \tag{52}$$

J is the Jacobean differential given by the formula:

$$J = \frac{\partial[F_1 F_2 F_3]}{\partial[VMP]} \tag{53}$$

$|H - \lambda I|\Omega_i = 0$ is the characteristic equation of the matrix of Eq. (50) from where the eigenvalues or the roots can easily be evaluated. In this way, the problem is decoupled into three-dimensional maps and the stability question is answered once the eigenvalues ($\lambda_{1k}, \lambda_{2k}, \lambda_{3k}$) for each iteration are known. If the Jacobeans are real and symmetric such that one would expect real eigenvalues, the system is asymptotically stable if $-1 < \lambda_{1k}, \lambda_{2k}, \lambda_{3k} < 1$, but unstable if λ_{1k}, λ_{2k}, $\lambda_{3k} > 1$ in absolute terms. If one of the eigenvalues λ_{1k} or λ_{2k} or λ_{3k} has modules equal to 1 in absolute value, then the critical point is established for stability. A leak in a pipeline causing instability is observed when the simulation results in at least one of the roots $\lambda_{1k}, \lambda_{2k}, \lambda_{3k} < -1$. Similarly, a surge causing instability is observed when at least one of the roots $\lambda_{1k}, \lambda_{2k}, \lambda_{3k} > 1$. The absolute value of 1 is the critical bifurcating state. If $\lambda_{1k}, \lambda_{2k}, \lambda_{3k}$ are such that, the Jacobean are complex conjugates (i.e. $\lambda_{1k}, \lambda_{2k}, \lambda_{3k} = \alpha + \mathrm{i}\beta$), the stability criterion for three-dimensional maps can be solved, where the system is stable (for complex conjugates) if all eigenvalues are inside the unit circle, whereas the system is asymptotically unstable, if at least one of the eigenvalues is outside the circle.

The stability boundary is the unit circle itself. If the eigenvalues are real there are only two points where they can cross the stability boundary at 1 and -1. This concept is similar to saying that the stability condition exist once the Jacobean is equal to 1 in absolute terms. In order to describe the unstable phase portrait, a bifurcation model to assign a relative magnitude to the disturbed phase is proposed, as the standard deviation from the critical point, which gives a robust measure of the width of distribution. These are indicated in Eqs. (54)–(56) for the eigenvalues:

$$\text{S.D.}(\lambda_{1ij}) = \sqrt{\sum_{i=0}^{n} \frac{(|\lambda_{1ij}| - 1)^2}{n-1}} \tag{54}$$

$$\text{S.D.}(\lambda_{2ij}) = \sqrt{\sum_{i=0}^{n} \frac{(|\lambda_{2ij}| - 1)^2}{n-1}} \tag{55}$$

$$\text{S.D.}(\lambda_{3ij}) = \sqrt{\sum_{i=0}^{n} \frac{(|\lambda_{3ij}| - 1)^2}{n-1}} \tag{56}$$

The standard deviation model evaluates the width of deviation of a typical flow vector point at time $i = 0, \ldots, n$. Once a leak is suspected at a time envelope, a relative magnitude of the disturbance can be ascertained. A standard deviation close to zero indicates a small leak, and vice versa. $|\lambda_{1ij}|$, $|\lambda_{2ij}|$, $|\lambda_{3ij}|$ are the absolute eigenvalue of velocity, mass and pressure, at a particular time and pipeline node point. Hence, using the standard deviation model, it is possible to classify the leak being considered. This model is useful for assigning a value to a disturbance after the eigenvalue criterion for a leak or surge has been ascertained.

5. Location of leak in a pipeline

When a leak occurs, the resulting leak wave travels at sonic velocity on the fluid [1]. The time lag between the instance when a leak is detected and when there is no leak is a measure of the time it takes the leak wave to travel the distance from the leak source to the sensors upstream and downstream. The distance traveled is evaluated by multiplying this time lag with the sonic velocity c thus

$$D_{\text{LU}} = c\Delta t_{\text{u}} \tag{57}$$

$$D_{\text{LD}} = c\Delta t_{\text{d}} \tag{58}$$

$$D_{\text{LA}} = \tfrac{1}{2}(D_{\text{LU}} + D_{\text{LD}}) \tag{59}$$

The sonic velocity is given by the following equation:

$$c = \sqrt{\frac{1}{((1/K_{\text{eff}}) + (DE_{\text{s}}/t_{\text{w}}))\rho}} \tag{60}$$

The leak size can be estimated from the magnitude of flow discrepancies. The leak location can also be determined by two possible methods [14]. They are

(i) least square fit of pressure profile,
(ii) the gradient intersection method.

The least square fit of pressure profile can be used in the manner described. Once a leak is indicated either by an identifiable pattern of flow discrepancies or deviations above mass balance thresholds, then a leak location search is initiated, where a leak is imposed to the location search procedure and the resulting pressure profile is checked against SCADA (Supervisory Control and Data Acquisition) measurements.

Whereas the gradient intersection method is used to locate a leak by a pseudo steady-state profile, which is calculated in the forward direction using pipe inlet conditions and in the reverse direction using pipe outlet conditions. A leak is located at the intersection of the hydraulic gradient lines. This method in particular relies on the expectation that a leak disturbance settles out eventually to a new steady-state position.

6. Certainty of a leak in a pipeline

The certainty of a leak in a pipeline is obtained by the number of votes that favor leak relative to the total number of votes in the operating window. In a typical pipeline, the possible situations of flow are stable systems, positive unstable systems (surge), and negative unstable flow system (leak), which render the subjective probability for any of

the events to happen to be 1/3 for each iteration. The occurrence of a leak is determined by the results of simulation of a computer program. Each time the computer program does an iteration to evaluate the eigenvalues; the activity is synonymous to a random probability experiment. The outcome of the simulation is the event of chance. If the eigenvalues have at least one of the roots λ_{1k}, λ_{2k}, λ_{3k} less than -1 a leak count is recorded. The number of iterations n, of the computer simulation is the total number of votes, whereas, the number m that favors leak is the number of times the outcome of simulation results in λ_{1k}, λ_{2k}, λ_{3k} less than -1. Baye's theorem can consequently be applied [5]. The probability that a leak has occurred is then given by the following equation:

$$P_{kj}(L) = \frac{P_{kjs}(L)}{P_{kjs}(L) + 2P_{kjs}(NL)} \tag{61}$$

Eq. (61) is the computed probability at a particular time for a particular node j, whereas $P_{kjs}(L)$ is the simulated probability (m/n). The overall probability for any simulation run

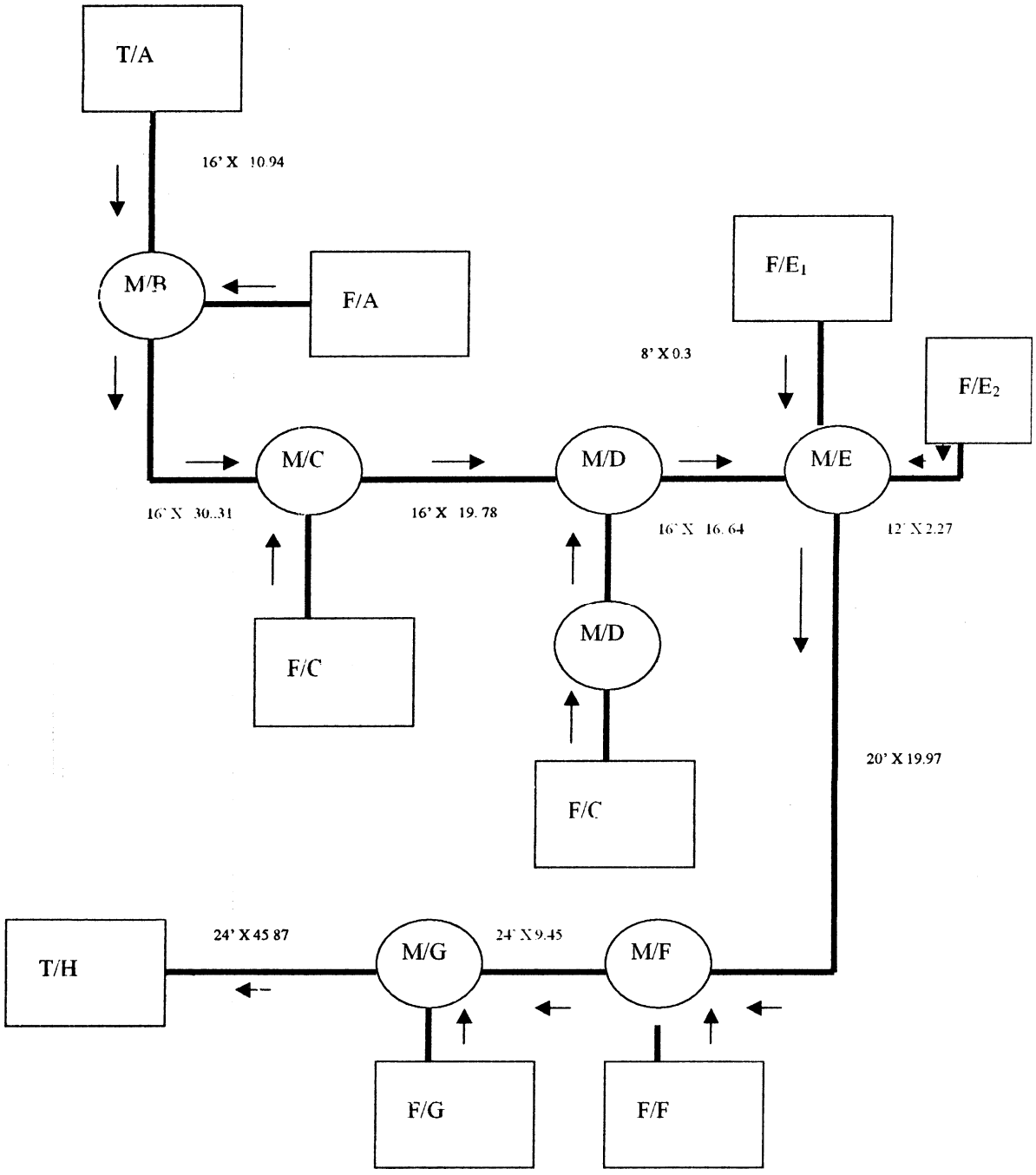

Fig. 1. Studied pipeline network system.

can be fitted into any of the probability distribution functions (normal distribution, gamma or Poisson) to see which distribution best predicts the observed trend.

7. Computeranalysis

A computer program was written to simulate the flow and leak of fluid in a pipeline system. A subroutine program leak track was developed to detect and *track leaks* in pipelines. The subroutine examines different leak or no leak status as discussed in Sections 4 and 5 above and locates the position of the leak when there is a deviation from equilibrium. A subroutine program developed is used to simulate the flow behavior.

Data supplied by pipeline operators was used to simulate the flow pressure and velocity within some specified pipeline segment. A flow diagram of the pipeline subnetwork considered is presented in Fig. 1. Figs. 2 and 3 show the flow chart, for simulating the flow and leak system. The leak and flow behavior of a crude petroleum pipeline (20 km) segment, of an operating pipeline network of an oil producing company in Nigeria was studied. The leak detection study was chosen for k_L factors that simulate the flow behavior. Different leak scenarios were represented by different leak factors.

8. Discussion of results

8.1. Plot of dynamic simulated pressure and velocity with pipeline distance at different times for $k_L = 0.0$ (no leak situation)

Figs. 4 and 5 show the dynamic simulated pressure and velocity profiles, respectively, for different time periods as functions of pipeline distance for no leak (i.e. $k_L = 0.0$), for studied pipeline segment of pipeline network. In Fig. 5, the velocity is constant for all process times, which shows that constant velocity plots indicate no leak. However, for no leak, the pressure profiles show slight deviation at different times, which can attributed to frictional and valve loses.

8.2. Plot of dynamic simulated pressure and velocity with pipeline distance at different times for $k_L = 1.5$ (leak situation)

For a leak factor $k_L = 1.5$ (Fig. 6), the slopes of the pressure plots were much larger than that in Fig. 4 (the no leak case) and the corresponding velocity profiles exhibit slight deviations from constancy (Fig. 7). In this case, velocity becomes a poor indicator of leak when the leak factor is small ($k_L = 1.5$).

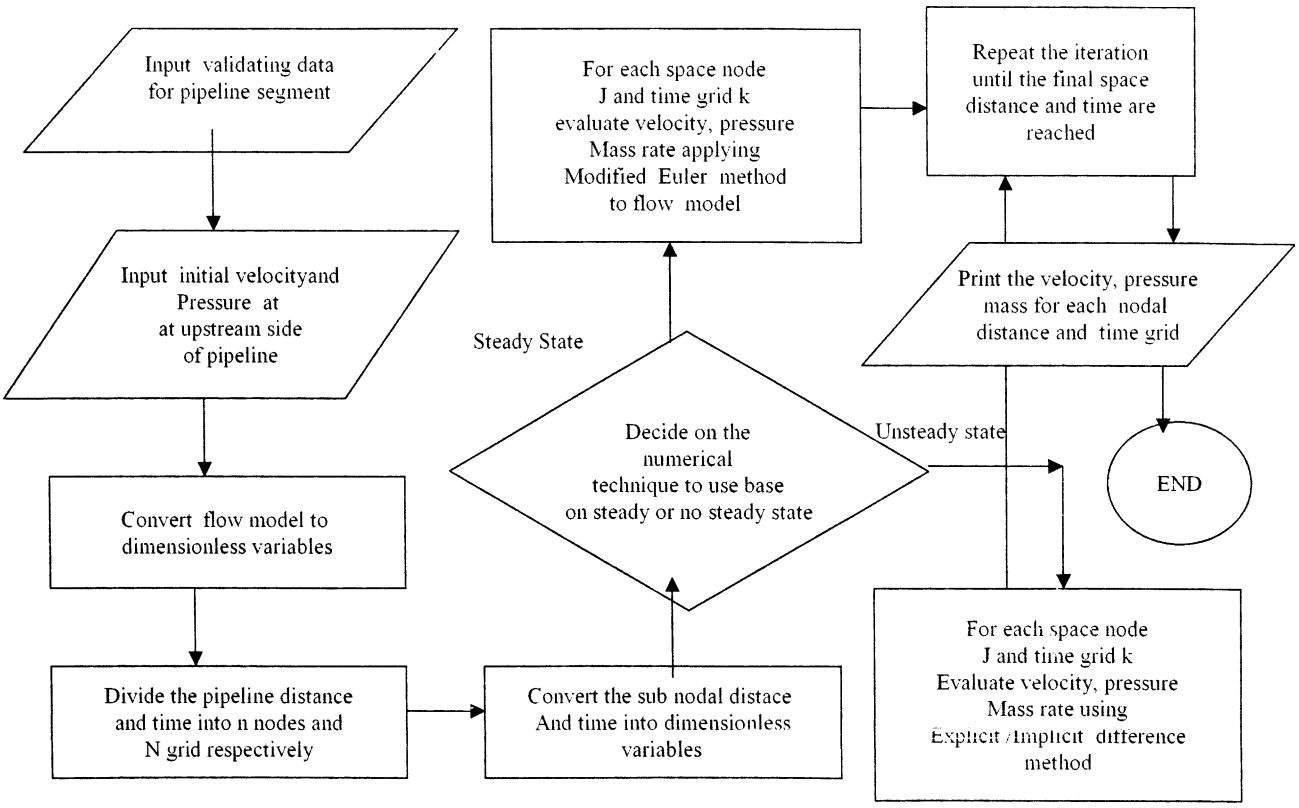

Fig. 2. Flow simulation chart.

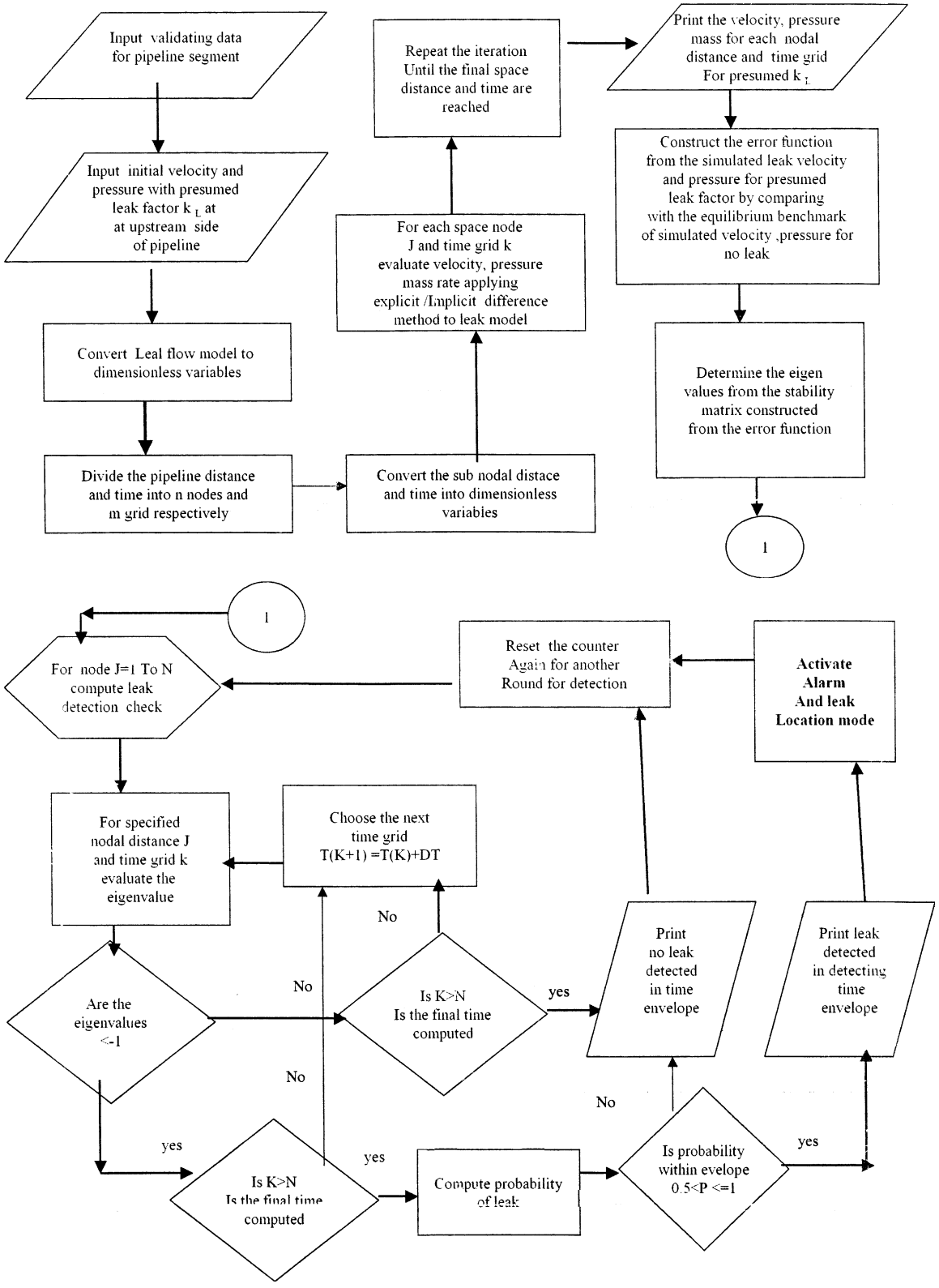

Fig. 3. Leak simulation chart.

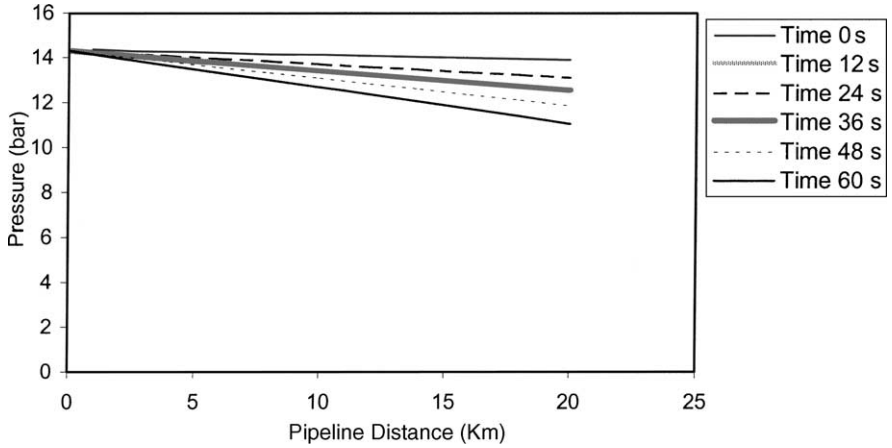

Fig. 4. Dynamic simulated pressure profile at various times for pipeline from Opukushi to Tunu M/F for leak situation.

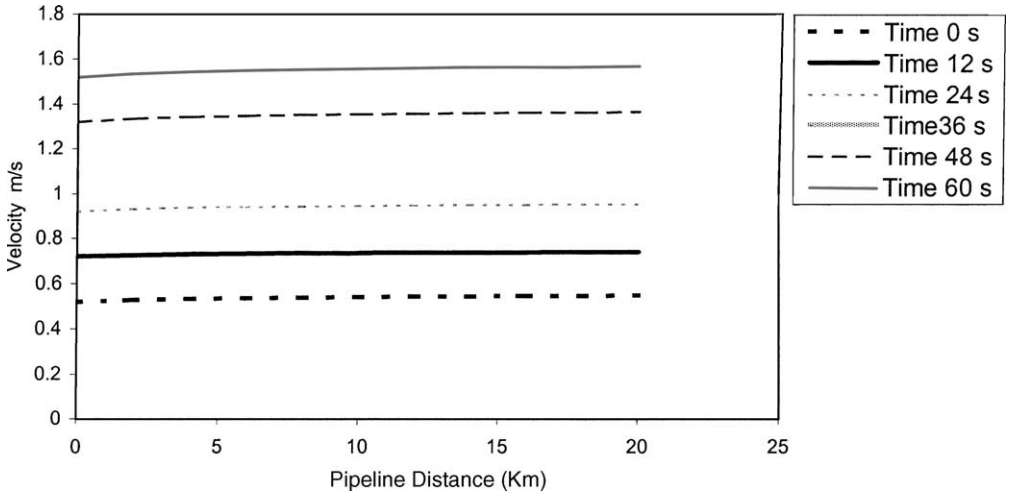

Fig. 5. Dynamic simulated velocity profile at various time for pipeline for Opukushi M/F to Tunu M/F without leak considerations.

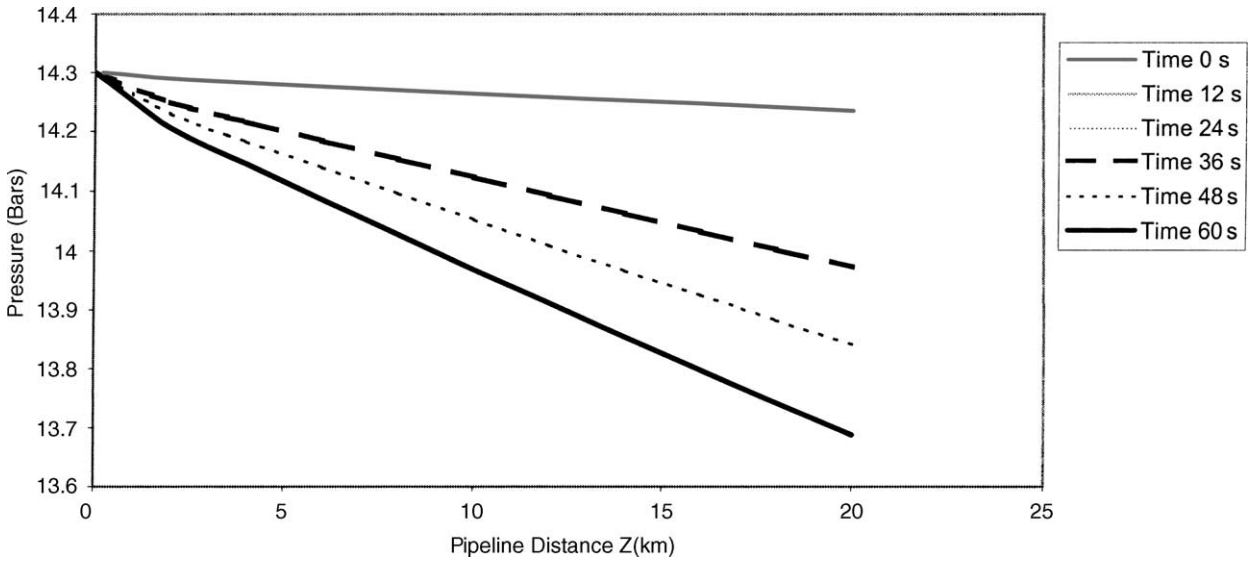

Fig. 6. Dynamic simulated pressure profile at various times of pipeline from Opukushi M/F to Tunu M/F with leak considerations $k_L = 1.5$.

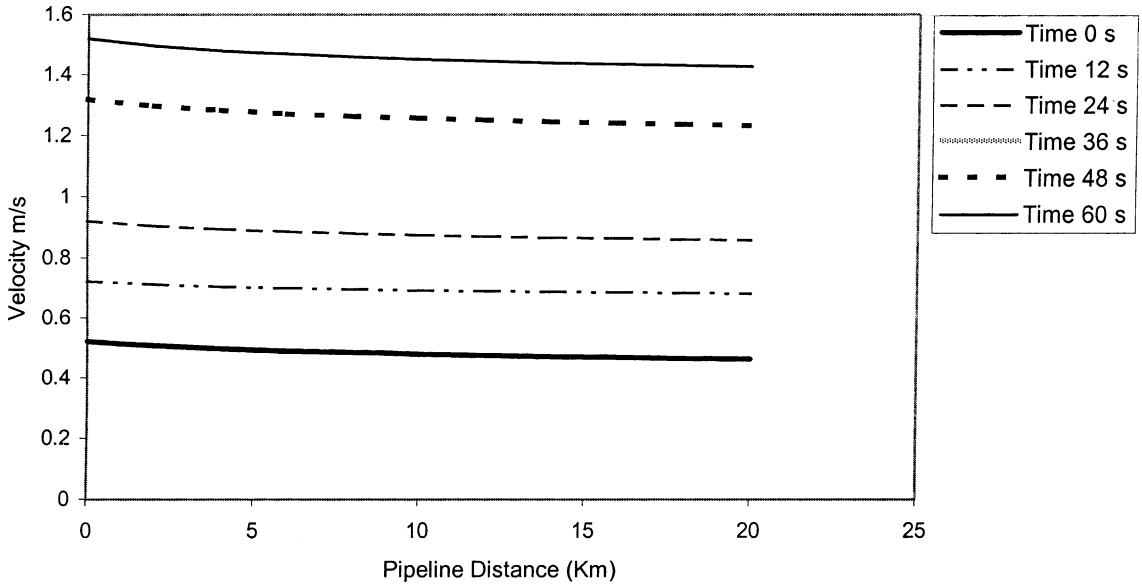

Fig. 7. Dynamic simulated velocity at various time for pipeline from Opukushi M/F to Tunu M/F with leak consideration $k_L = 1.5$.

8.3. Plot of dynamic simulated pressure and velocity with pipeline distance at different times for $k_L = 3.0$ (leak situation)

The pressure profiles (see Fig. 8 at $k_L = 3.0$) show more significant deviations than the case for $k_L = 1.5$. However, for larger leak factor, $k_L = 3.0$ (Fig. 9), the velocity profiles deviated significantly from the constant values characterizing no leak ($k_L = 0$) and relatively small leak ($k_L = 1.5$). Thus, the leak model used here to predict leak behavior indicates that the pressure measurements are more sensitive parameters for leak detection. The volume measurements appear to be only slightly more sensitive indicators for larger leak systems. These trends are well supported by Leitko [6], for long pipelines.

8.4. Plot of eigenvalue pressure and velocity with time for $k_L = 1.5$ and $k_L = 3.0$ (leak situation) at different node distance of pipeline segment

We will now compare the velocity and pressure profiles with their corresponding eigenvalues as indicators for leak

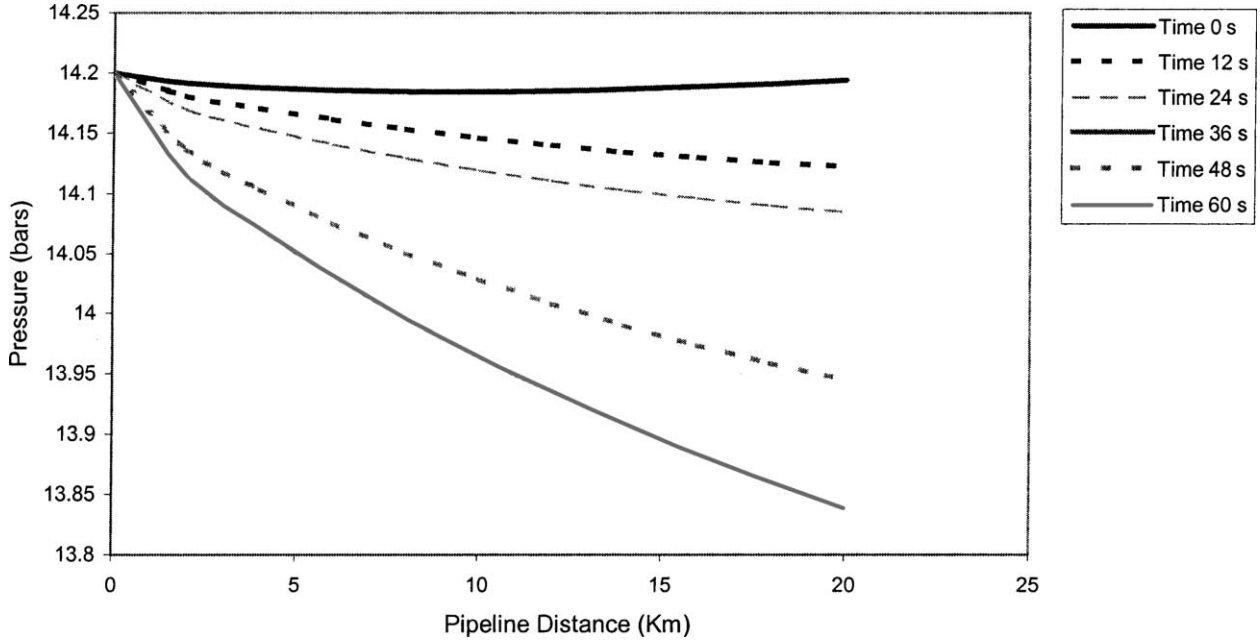

Fig. 8. Dynamic simulated pressure profile at various times of pipeline from Opukushi M/F to Tunu M/F with leak considerations at $k_L = 3.0$.

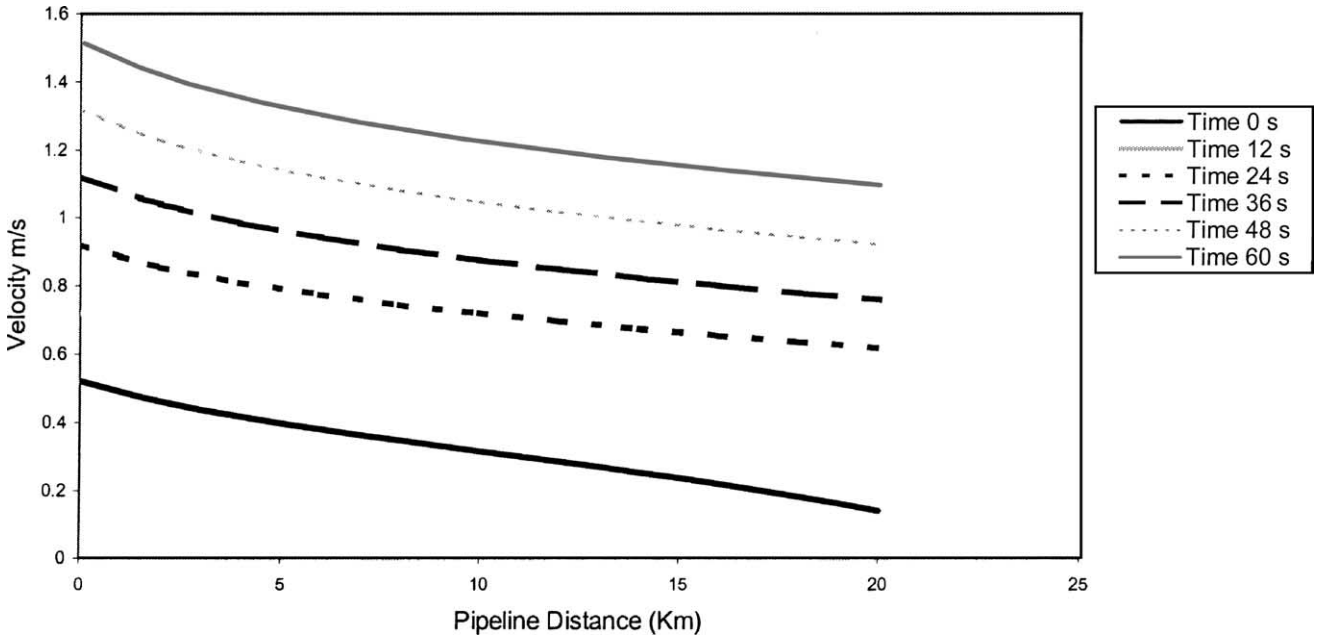

Fig. 9. Dynamic simulated velocity at various times of pipeline from Opukushi M/F to Tunu M/F with leak considerations at $k_L = 3.0$.

detection. Are the eigenvalue plots more sensitive parameters for leak detection than their corresponding pressure and volume measurements?

Fig. 10 shows plots of eigenvalues with time for pressure measurements. The pressure waveform oscillates in the negative portion of the *x–y* plot. The waveform moves from a critical point of 1 (stable point) to an unstable position in the negative part of the plot, exceeding the value of −1 (critical leak point) after 4 s. The clustering of the waveform is indicative of a small leak. However, for larger leak system, $k_L = 3.0$ (Fig. 11), the waveform is more pronounced, having larger amplitude. The separation of clustering of the waveform is well defined. The waveform as before moves from a critical surge point of 1 to an unstable leak position in the negative region, typical of large leak systems.

However, the observed trend is slightly different for plots of eigenvalue velocity with time for volume measurement. Fig. 12 shows profiles of eigenvalue with time for a leak factor of $k_L = 1.5$ at different pipeline distance. The fact that the waveform of all profiles shifted from a critical value of 1

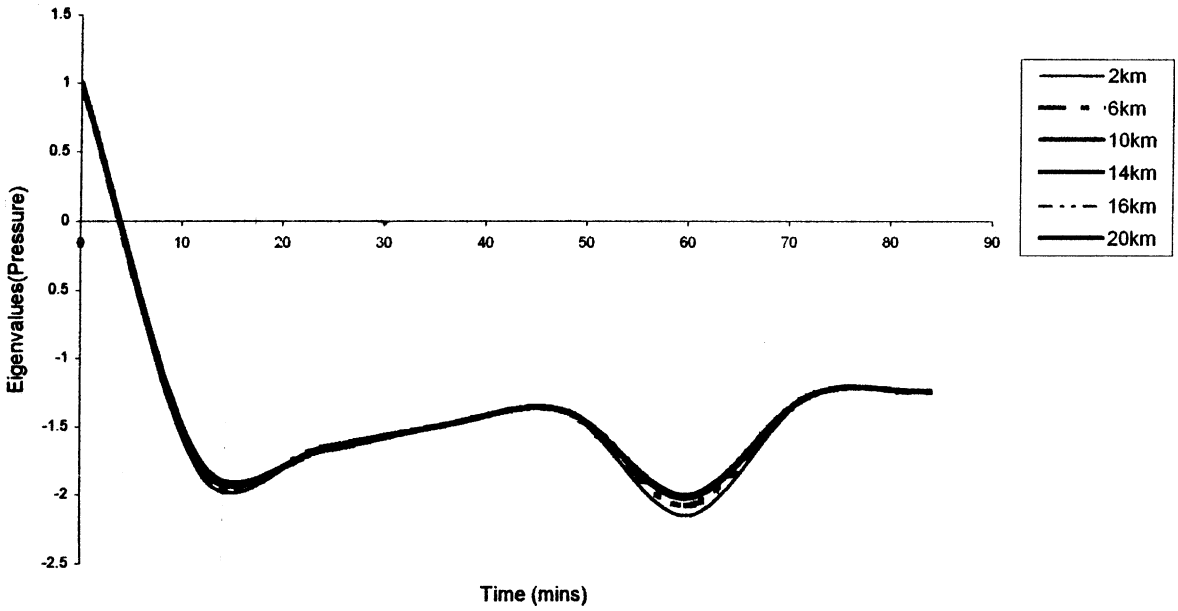

Fig. 10. Eigenvalues with time at various distance with leak factor $k_L = 1.5$ for pipeline from Opukushi M/F to Tunu M/F.

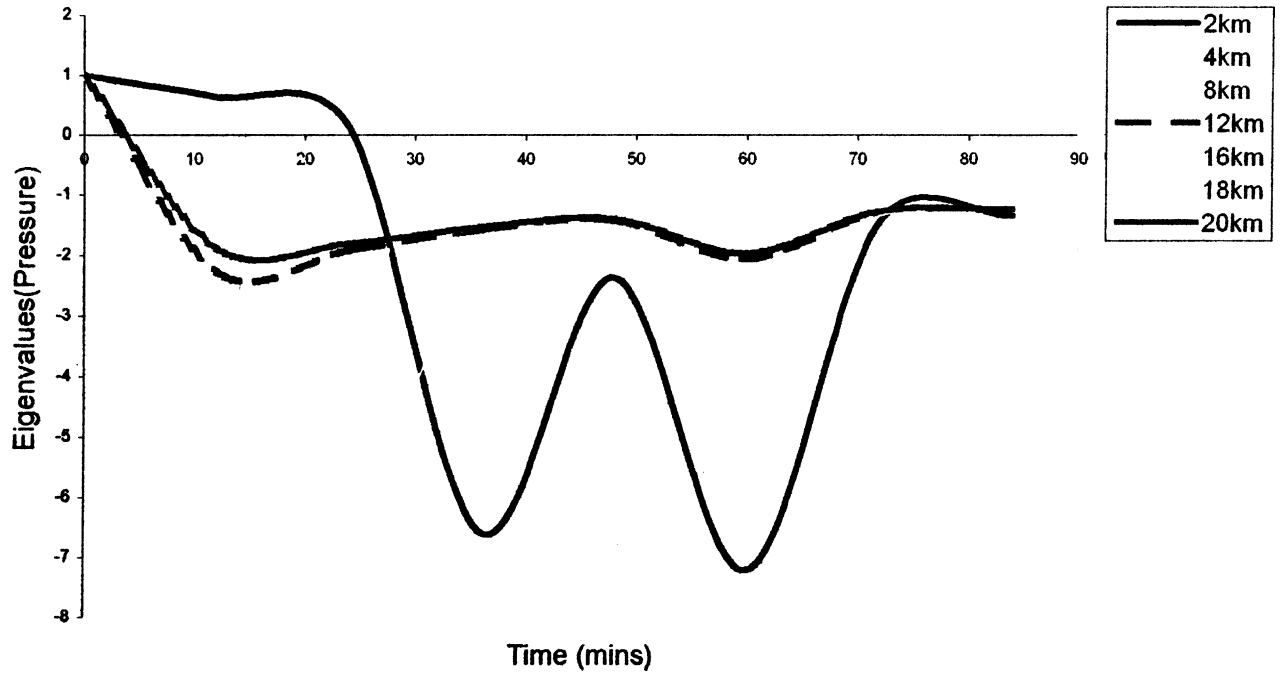

Fig. 11. Eigenvalues (pressure) against time at various pipeline distance for a leak factor $k_L = 3.0$ for pipeline from Opukushi M/F to Tunu M/F.

to below −1, attaining a minimum at eigenvalue velocity of −1.5 at time 25 s, clearly indicates that a leak has occurred. Fig. 13 shows a more interesting behavior. The eigenvalue velocity profiles with time for leak factor $k_L = 3.0$ at specific distance nodes, show waveforms that are exponential in character and there was no significant deviation from the case where the leak factor $k_L = 1.5$. This again confirm that velocity measurements are less sensitive parameters for leak detection when compared with pressure measurement.

8.5. Plot of eigenvalue velocity with pipeline distance for studied pipeline network at different times for different leak factors $k_L = 1$–5

In this section, we shall show that by using eigenvalue vs. distance plots; we can locate the source of leaks.

Figs. 14–16 show the plots of eigenvalue velocity with pipeline distance for different leak factors at times 24, 48 and 72 s for leak occurring at a point that is located at 1 km

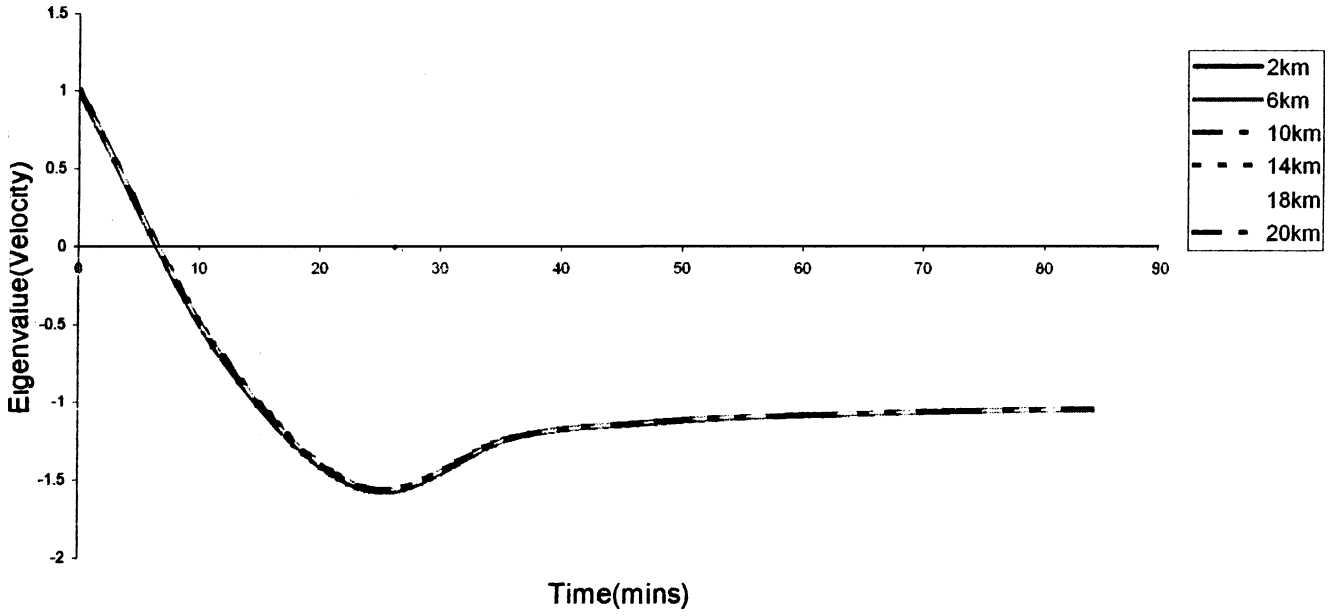

Fig. 12. Eigenvalue (velocity) against time for leak factor $k_L = 1.5$ at various pipeline distance for pipeline from Opukushi M/F to Tunu M/F.

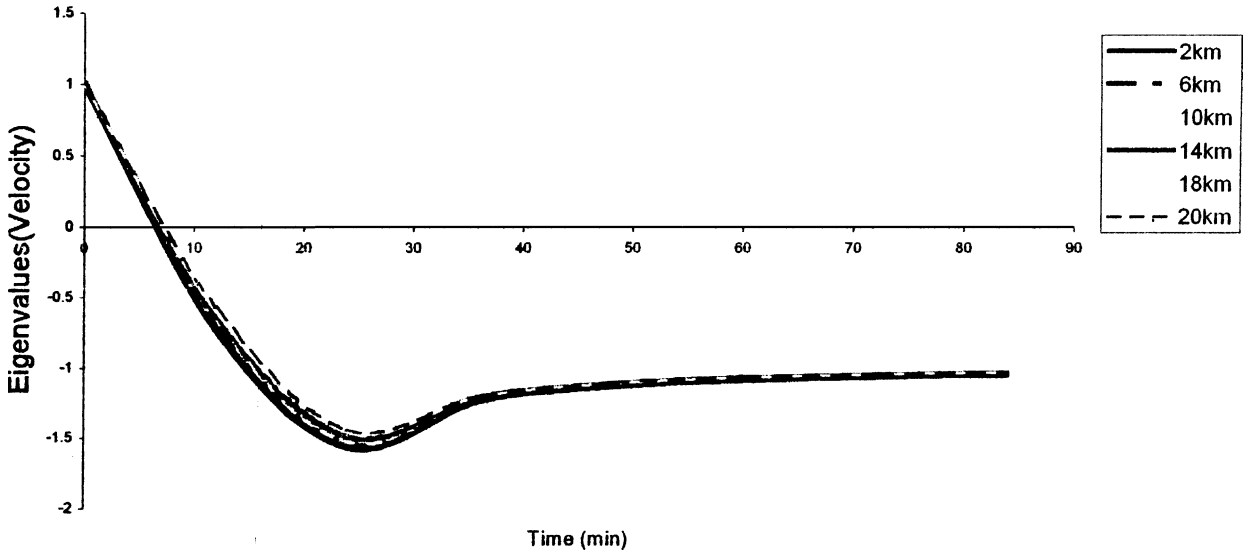

Fig. 13. Eigenvalue (velocity) against time for leak factor $k_L = 3.0$ at different pipeline distance for pipeline from Opukushi M/F to Tunu M/F.

from the end of the pipe at an upstream location. It is obvious from these plots that the oscillatory behavior of the waveform is more pronounced for small leaks signified by small leak factors than for larger leaks signified by larger leak factors at specific time measurement. For example, the cluster between waveforms of different leak factors becomes more distinct with time (compare Figs. 14–16). The sinusoidal waveforms, characteristic of the eigenvalue behavior, are so prominent in Figs. 15 and 16 (see Sections 8.2 and 8.3). The sinusoidal waveform becomes more defined as time progress, as revealed in Figs. 14–16. These waveforms allow us to characterize and locate the source of the leak. This is so, because the waveforms can be used to evaluate the propagation velocity of the particular leak factor scenario, from where the distance of the leak can be determined by the product of the propagation velocity and the instantaneous leak time deviation. The instantaneous leak time deviation is the deviation in time that has elapsed, between the last measurements that indicated no leak and the next measurement that indicated a leak.

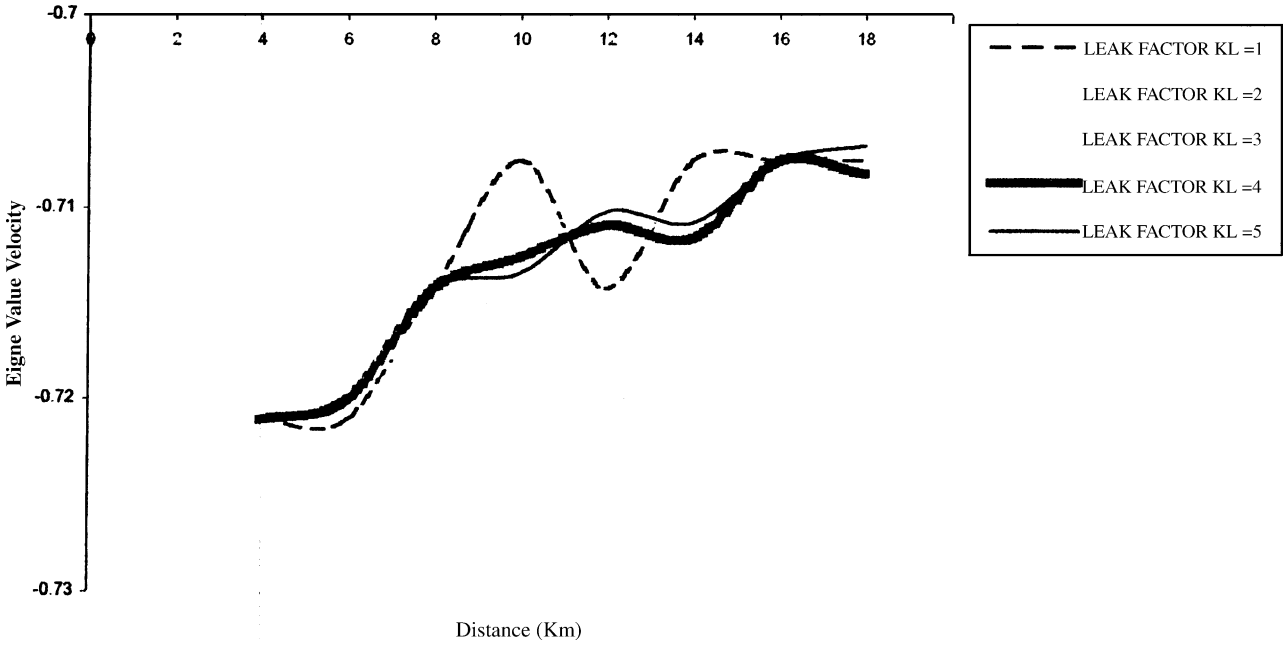

Fig. 14. Plot of velocity eigenvalues with pipeline distance for studied pipeline network system at 24 s simulated time.

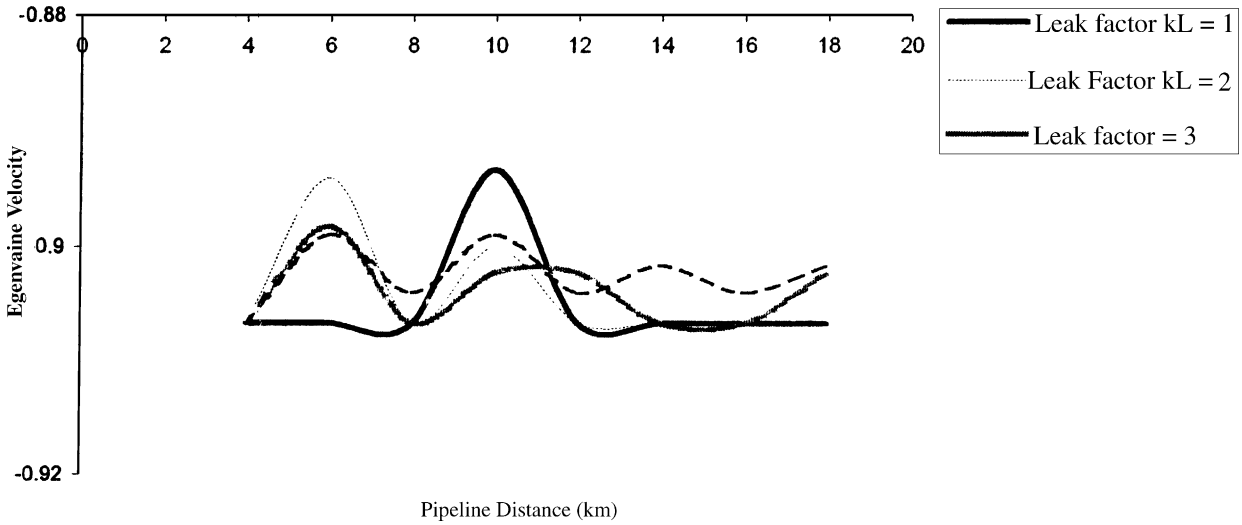

Fig. 15. Plot of eigenvalue velocity with pipeline distance for studied pipeline segment for different leak factor at 48 s.

8.6. Plot of eigenvalue pressure with pipeline distance for studied pipeline network at different times for different leak factors $k_L = 1$–5

We shall now explore eigenvalue pressure vs. distance plots to compare the behavior with the velocity vs. distance plots described in Section 8.4. This comparison will determine which of the two plots would be superior for the location of a leak.

Figs. 17–19 show the plot of eigenvalue pressure with pipeline distance for different leak factors for leak located at a point 1 km from the end of the pipe at a downstream location. These plots exhibit for different leak factors interesting trends, as the waveform is exponential for a specific eigenvalue interval (i.e. eigenvalue increase between −1.31 and −1.27, for leak factor $k_L = 1$), and assumes oscillatory behavior afterwards. As the leak factor decreases, the trend is towards higher eigenvalues. The waveforms exhibited here are unique and distinct and are easily distinguishable from the portrayals by the eigenvalue velocities (see Section 8.4).

However, as time progresses, as revealed in Figs. 18 and 19, the maximum peaks become more defined and the separation between the waveforms become larger when compared with Fig. 17. Furthermore, the behavior after the maxima showed less oscillation. A simple explanation of this behavior is now proposed. As time progresses, the leak

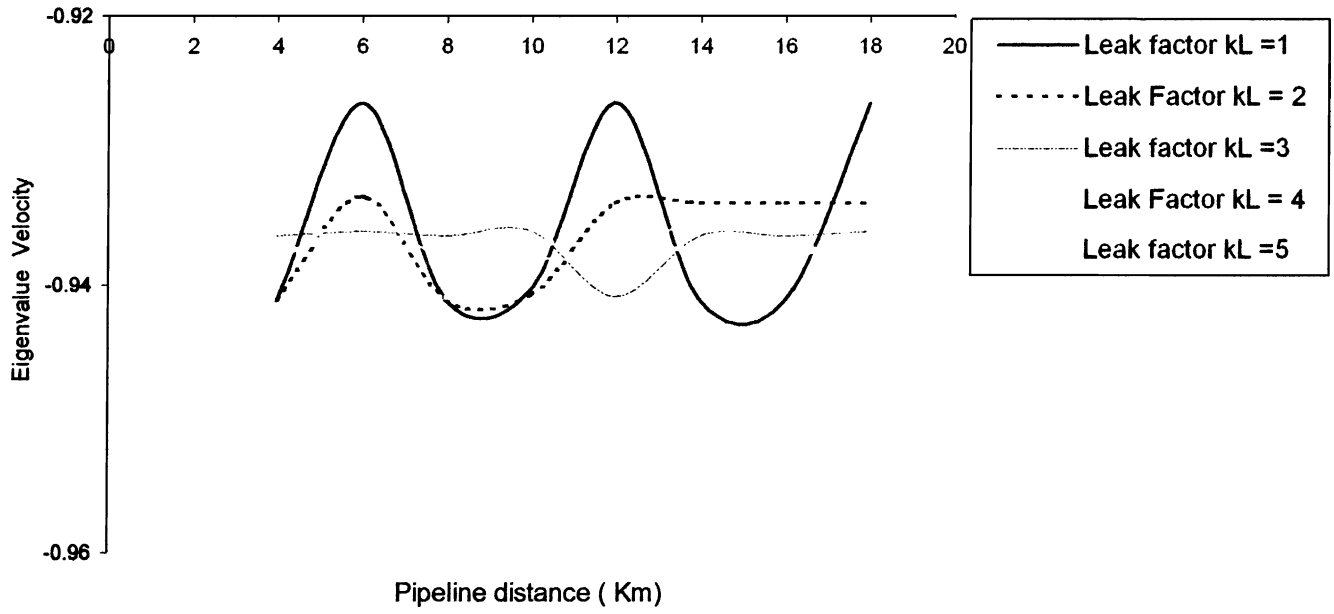

Fig. 16. Plot of eigenvalues velocity for different leak factor with time at 72 s.

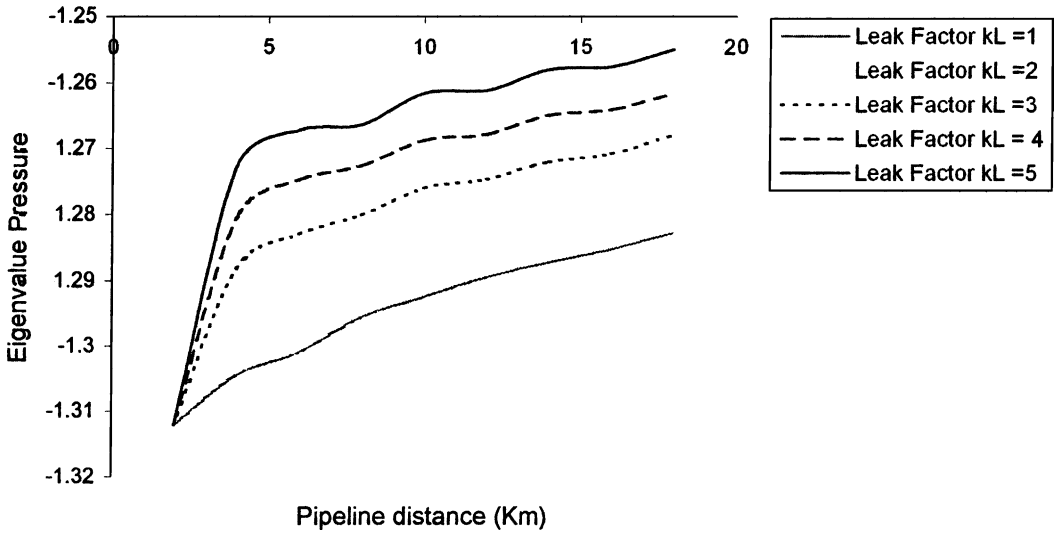

Fig. 17. Plot of eigenvalue pressure with pipeline distance for different leak factor at time 24 s.

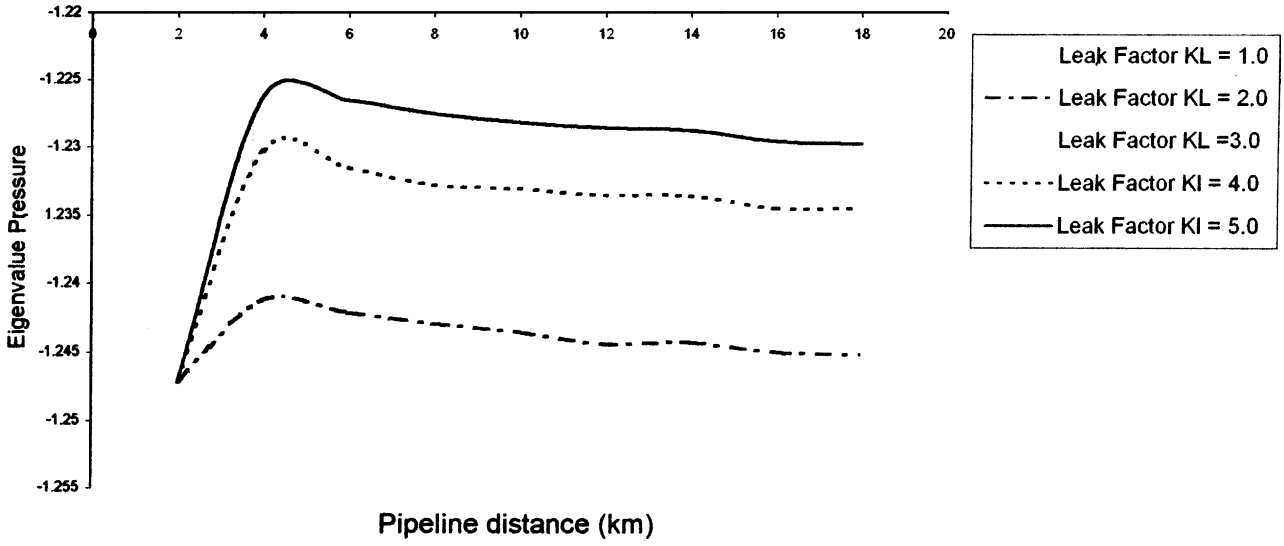

Fig. 18. Plot of eigenvalue pressure with pipeline distance for different leak factor at $k_L = 48$ s.

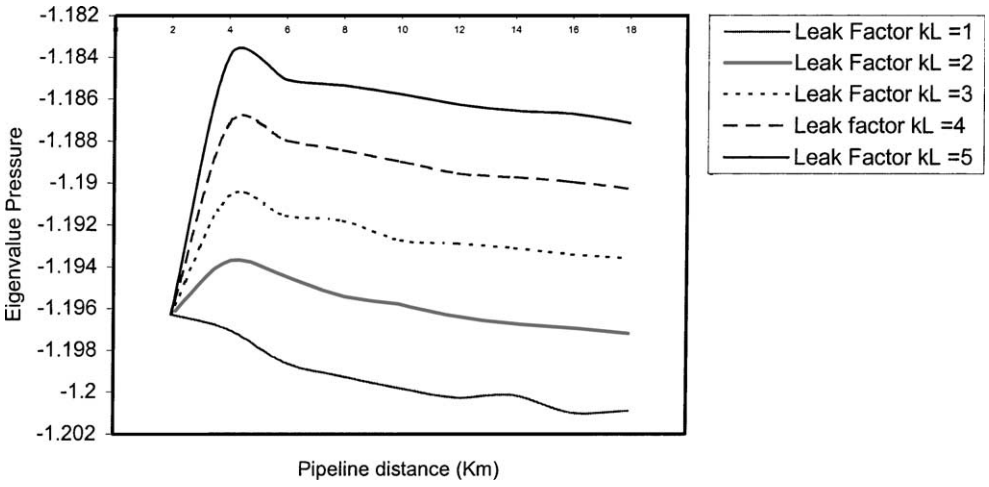

Fig. 19. Plot of eigenvalue pressure with distance for different leak factor for studied pipeline segment at 72 s.

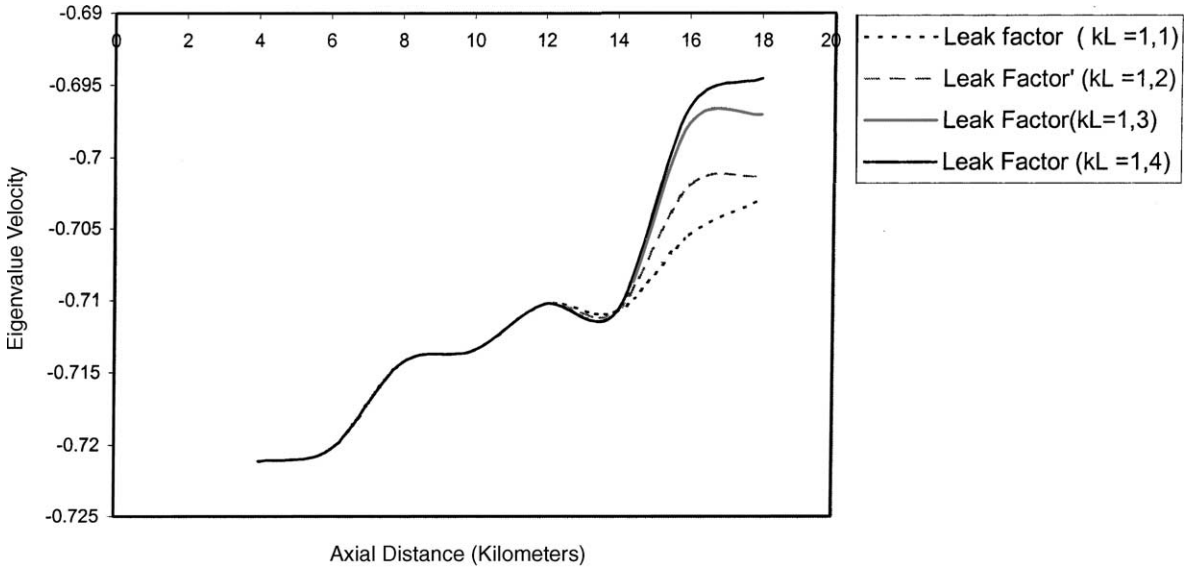

Fig. 20. Plot of eigenvalues with distance for leak factor $k_L = 1$ at 1 km from upstream side and $k_L = 1$ at 1 km from downstream for time 24 s.

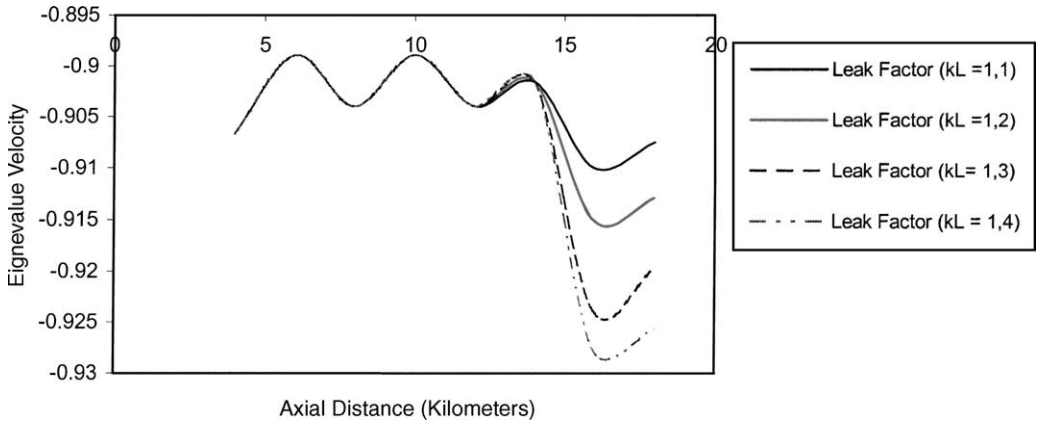

Fig. 21. Plot of eigenvalue velocity with axial distance at time 48 s for leak factor at 1 km from pipeline downstream and upstream side for studied pipeline segment.

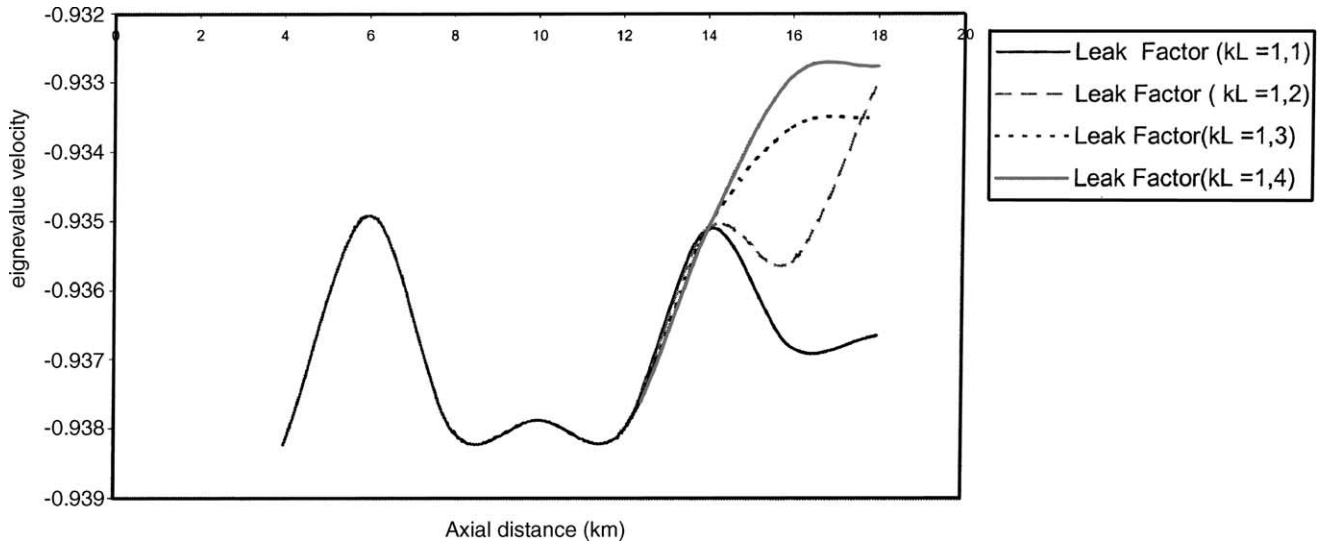

Fig. 22. Plot of eigenvalue velocity with axial distance for different leak factor 1 km upstream and downstream at time 72 s for studied pipeline segment.

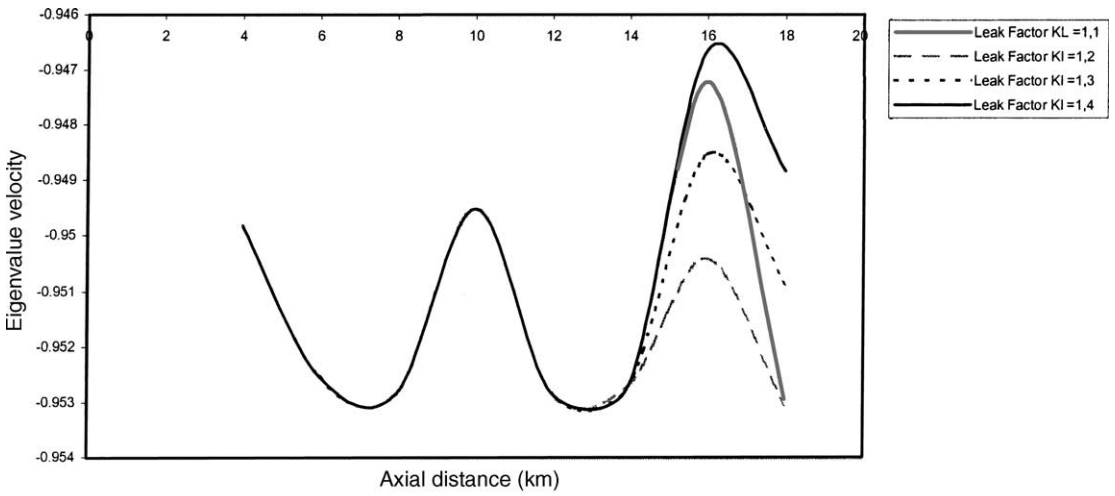

Fig. 23. Plot of eigenvalue velocity with axial velocity for different leak factor at leak distance 1 km upstream and downstream for time 96 s.

waveforms equilibrate from unsteady to steady situation. These are the characterizing trends of eigenvalue pressure with pipeline distance at different leak factor situations. It can be deduced that pressure measurements are more reliable parameters for leak detection than velocity measurements. In addition, the relative magnitude of the eigenvalue velocity plots is in the neighborhood that is less than −1. Although this is located in the negative region, it is not sufficient to confirm a leak as such. In comparison, eigenvalue pressure profiles exhibit eigenvalues that are much greater in magnitude than −1. Thus, the pressure would be a more preferable index of locating a leak. Again, it is possible to locate the leak in a pipeline by evaluating the propagating velocity from the waveform and multiplying it by the instantaneous leak time deviation.

8.7. Plot of eigenvalue velocity with distance with two leaks, one 1 km from upstream end of the pipeline with $k_L = 1$ and the other leak at 1 km downstream at the end of the pipeline with varying k_L's

So far, we have been concerned with a single leak in a pipeline system. What will happen if there exist a leak at a location 1 km from one end of a pipeline and another leak located at 1 km from the other end of the pipe? If the upstream leak has a constant $k_L = 1$, what then happens to the leak located at the downstream end if its k_L factors are varied significantly? We shall explore this with the eigenvalue velocity plots and compare the results of this analysis with the eigenvalue pressure plots in Section 8.8.

Figs. 20–23 show the plot of eigenvalue velocity with distance for two leak points, 1 km from upstream end of the

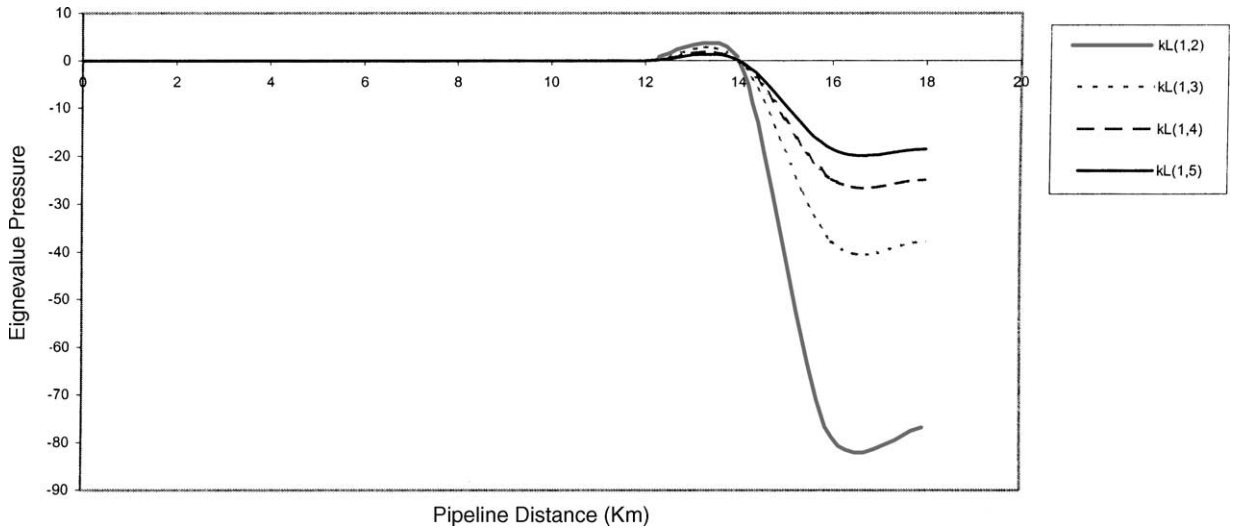

Fig. 24. Plot of eigenvalue pressure with distance for different leak factors for time = 24 s for leak at 1 km upstream and downstream.

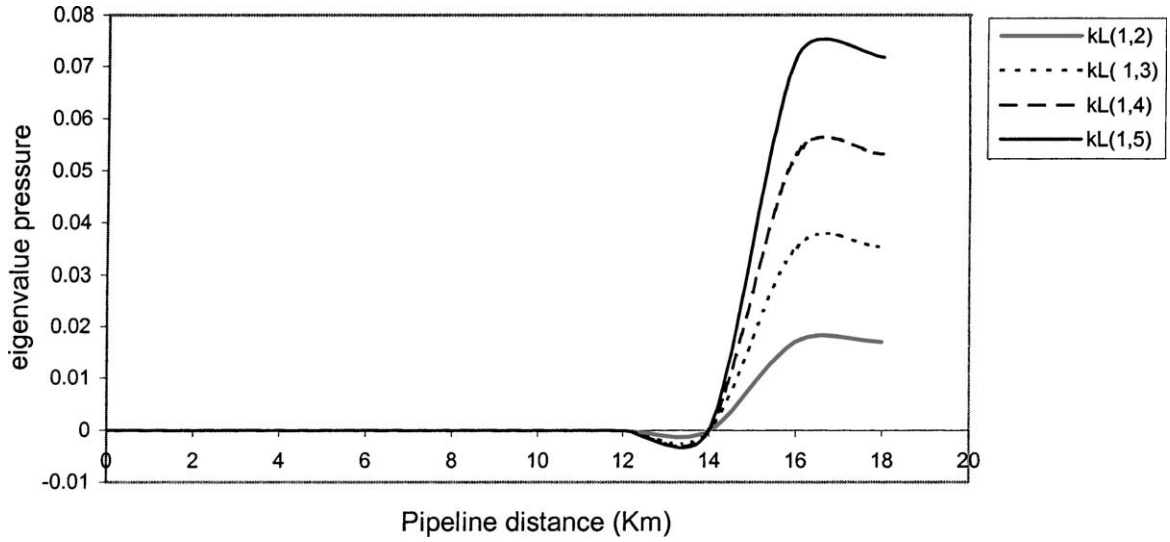

Fig. 25. Plot of eigenvalue pressure with distance for different leak factor for leak at 1 km upstream and downstream for time = 48 s.

pipeline and 1 km from downstream end of the pipeline. The upstream leak has a leak factor of $k_L = 1$, while k_L factor for the downstream leak is varied. The plots show that all waveforms for the different leak situations converge to one waveform up to a particular distance 14 km away from upstream, from where they diverge and become different waveforms. From the point of divergence, it is now possible to identify the individual waveforms. The leak factor $k_L = 4$ at 1 km from downstream side exhibit the largest maximum peak at time 24 s, the lowest minimum peak a time 48 s, the largest maximum peak for coordinates ($k_L = 1.4$) and the least minimum peak for coordinates ($k_L = 1.2$), at time 72 s, and a largest maximum peak for ($k_L = 1.5$) at time 96 s. These erratic trends in maxima can be attributed to the sensitivity of the velocity measurements. These trends are the characterizing leak behavior for two leak points. It is possible to locate the leaks from the behavior of the waveforms and the evaluation of the propagating leak velocity from the waveform. The product of the propagating leak velocity and the instantaneous leak time deviation now locates the leak.

8.8. Plot of eigenvalue pressure with distance with two leaks, one 1 km from upstream end of the pipeline with $k_L = 1$ and the other leak at 1 km downstream of the end of the pipeline with varying k_L

Figs. 24–27 show the eigenvalue pressure waveform with distance for different leak situations at different times, applicable for two leaks as described in Section 8.7. It is obvious that during the initiation of a leak, that is at 24 s, the

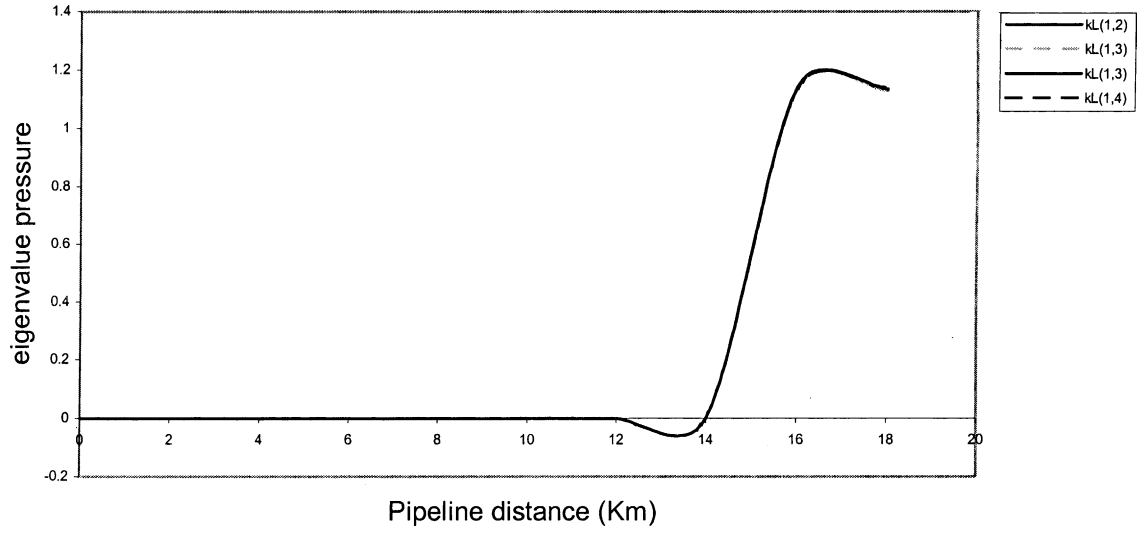

Fig. 26. Plot of eigenvalue pressure with distance for different leak factor for leak at 1 km downstream and upstream for time 72 s.

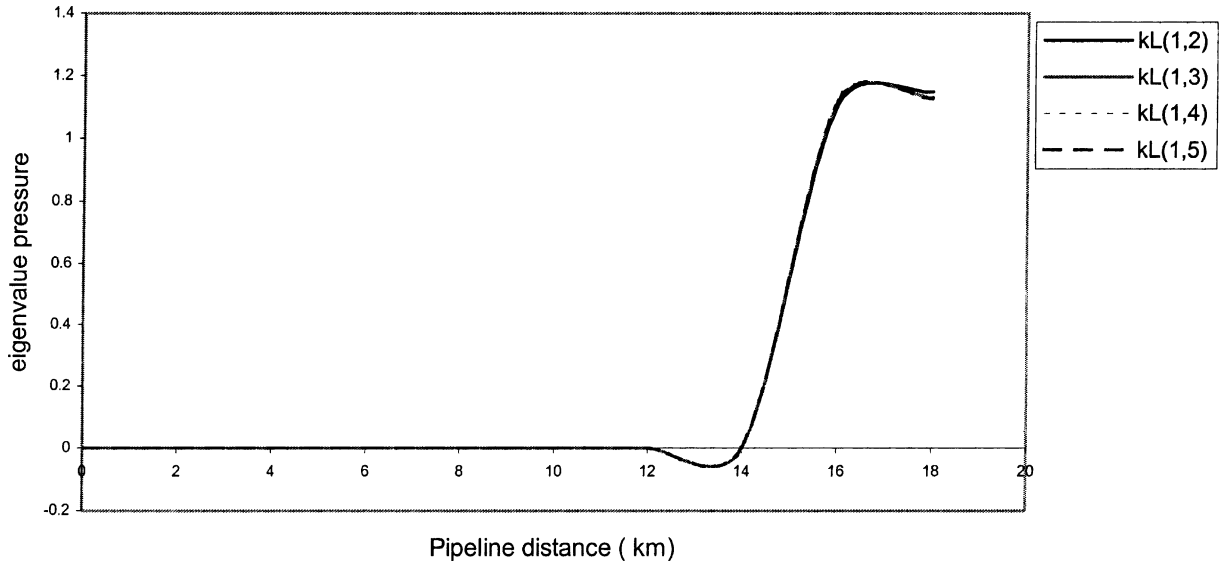

Fig. 27. Plot of eigenvalue pressure with distance for different leak factor for leaks at 1 km from upstream and downstream end for time 96 s.

eigenvalues were all negatives for all leak factors, with the minimum point reaching as much as −76 for leak factor k_L (1, 2). This is far in excess of what was obtained for eigenvalue velocity waveform. The fact that the eigenvalue is negative and large suggests that a leak waveform with large amplitude is occurring in the pipeline system. However, a different waveform emerges as time progresses. At 48 s, the waveform reverses making all eigenvalues positive with the waveform of k_L (1, 5), having the maximum peak. At 72 and 96 s, however, the waveform for all leak factors combined to give a single waveform. It may seem that this is the characterizing behavior for a situation with more than one leak. The reversal in waveform for pressure measurements may be due to the interference of the waveforms of leak waves from leak point locations 1 km upstream and downstream of the pipeline.

9. Conclusions

The following conclusions can be deduced from the discussion of results:

(i) Pressure measurements are more sensitive parameters for leak detection than volume measurements.
(ii) The constancy of the plots for velocity measurements against time indicates a no leak situation with slight deviation for small leak; larger deviations were observed for large leak systems.
(iii) The Liapunov concept of stability for predicting leak behavior was found suitable for describing leak systems. All the eigenvalues with time at various pipeline distance were all negative beyond −1 indicating a leak.
(iv) The sinusoidal waveform characterizes leak behavior for pressure measurements, whereas the exponential waveform characterizes velocity measurement.
(v) The waveform for eigenvalue with distance shows that pressure measurement have more distinct leak wave patterns than velocity measurement.
(vi) The waveform for the two leak case shows that the velocity and pressure waveforms for different leak situations combine up to 14 km from where they separate and exhibit more distinct waveforms.
(vii) The reversal in waveform for the eigenvalue pressure plots for the two leak cases may be explained by the interfering effect of the two waveforms emanating from the two leak sources located in the upstream and downstream ends of the pipeline system.

References

[1] E.W. Allister, Pipeline Rules of Thump Handbook: A Manual for Quick, Accurate Solutions to Everyday Pipeline problems, 2nd ed., Gulf Publishing House, Houston, Texas, 1988.
[2] R.B. Bird, W.E. Stewart, E.N. Lightfoot, Transport Phenomena, 2nd ed., Wiley, New York, 1960.
[3] G. Griebenow, M. Mears, Leak Detection Implementations: Modeling and Tuning Methods, vol. 19, American Society of Mechanical Engineers, Petroleum Division, 1988, pp. 9–18.
[4] A. Hamande, S. Cie, J.S. Sambre, New system pinpoints leaks in ethylene pipeline, Pipeline Gas J. 222 (4) (1995) 38–41.
[5] L.L. Lawrence, Probability and Statistics for Modern Engineering, 2nd ed., McGraw-Hill, New York, 1990.
[6] A.D. Leitko, Pressure point analysis: evaluation of Ed Farmer and Associates' Leak detection System, Shell Technical progress report WRC 330-88, EP 89 1109, 1989.
[7] J.C.P. Liou, J. Tian, Leak Detection: A Transient Flow Simulation Approach, vol. 60, American Society of Mechanical Engineers, Petroleum Division, 1994, pp. 51–58.
[8] C.R. Mauver, Buckeye's Long Island pipeline enhances leak detection, Oil Gas J. 9 (1991) 91–93.
[9] M.N. Mears, Real world applications of pipeline leak detection, pipeline infrastructure 11, in: Proceedings of the International Conference, ASCE, 1993.

[10] J.L. Modisette, Yellowstone Pipeline Leak Detection, Lic Energy Presentation Document, 1997.
[11] B. Parry, R. Mactaggart, C. Toerper, Compensated volume balance leak detection on a batched LPG pipeline, in: Proceedings of the Offshore Mechanics & Artic Engineering Conference, OMAE, 1992.
[12] L. Prandtl, Anger Math, Mechatronics 5 (1925) 136.
[13] Production Handbook, vol. 8, Pipelines, Shell Internationale Petroleum Maatschappij, The Hague, 1991.
[14] RELI, A Review of Pipeline Leak Detection Methods, REL Instrumentation project report, prepared for Shell International Exploration and Production Limited, March 1997.
[15] H. Schlichting, Boundary Layer Theory, McGraw-Hill, New York, 1955.
[16] J.N.T. Thompson, H.B. Stewart, Nonlinear Dynamics and Chaos—Geometrical Methods for Engineers and Scientist, Wiley, New York, 1989.
[17] M.C. Turner, Hardware and software techniques for pipeline integrity and leak detection monitoring, in: Proceedings of the Offshore Europe 1, Aberdeen, Scotland, 1991.
[18] Shell DEP Publications, Shell Internationale Petroleum Maatschappij, The Hague, 1994.